

**AFRL-VA-WP-TR-2000-3042**

**DEVELOPMENT OF THE  
AERODYNAMIC/AEROSERVOELASTIC  
MODULES IN ASTROS**

**VOLUME III - AEROSERVOELASTICITY DISCIPLINE IN  
ASTROS APPLICATION MANUAL**

**ZONA TECHNOLOGY INC  
7434 E STETSON DR SUITE 205  
SCOTTSDALE AZ 85251**



**FINAL REPORT FOR 9/1/96 -- 9/30/98**

**Approved for public release; distribution unlimited.**

**Air Vehicles Directorate  
Air Force Research Laboratory  
Air Force Materiel Command  
Wright-Patterson AFB, OH 45433-7542**

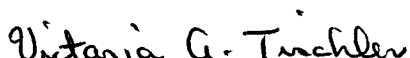
**20001113 082**

## NOTICE

USING GOVERNMENT DRAWINGS, SPECIFICATIONS, OR OTHER DATA INCLUDED IN THIS DOCUMENT FOR ANY PURPOSE OTHER THAN GOVERNMENT PROCUREMENT DOES NOT IN ANY WAY OBLIGATE THE UNITED STATES GOVERNMENT. THE FACT THAT THE GOVERNMENT FORMULATED OR SUPPLIED THE DRAWINGS, SPECIFICATIONS, OR OTHER DATA DOES NOT LICENSE THE HOLDER OR ANY OTHER PERSON OR CORPORATION; OR CONVEY ANY RIGHTS OR PERMISSION TO MANUFACTURE, USE, OR SELL ANY PATENTED INVENTION THAT MAY BE RELATED TO THEM.

THIS REPORT IS RELEASEABLE TO THE NATIONAL TECHNICAL INFORMATION SERVICE (NTIS). AT NTIS, IT WILL BE AVAILABLE TO THE GENERAL PUBLIC, INCLUDING FOREIGN NATIONS.

THIS TECHNICAL REPORT HAS BEEN REVIEWED AND IS APPROVED FOR PUBLICATION.

  
VICTORIA A. TISCHLER

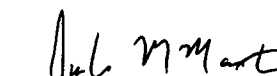
Aerospace Engineer

Structural Design and Development Branch

  
NELSON D. WOLF, Chief

Structural Design and Development Branch

Structures Division

  
JOSEPH M. MANTER, Chief

Structures Division

Air Vehicles Directorate

COPIES OF THIS REPORT SHOULD NOT BE RETURNED UNLESS RETURN IS REQUIRED BY SECURITY CONSIDERATIONS, CONTRACTUAL OBLIGATIONS, OR NOTICE ON A SPECIFIED DOCUMENT.

REPORT DOCUMENTATION PAGE			Form Approved OMB No. 0704-0188	
Public reporting burden for this collection of information is estimated to average 1 hour per response, including the time for reviewing instructions, searching existing data sources, gathering and maintaining the data needed, and completing and reviewing the collection of information. Send comments regarding this burden estimate or any other aspect of this collection of information, including suggestions for reducing this burden, to Washington Headquarters Services, Directorate for Information Operations and Reports, 1215 Jefferson Davis Highway, Suite 1204, Arlington, VA 22202-4302, and to the Office of Management and Budget, Paperwork Reduction Project (0704-0188), Washington, DC 20503.				
1. AGENCY USE ONLY (Leave blank)		2. REPORT DATE FEBRUARY 04, 1999	3. REPORT TYPE AND DATES COVERED FINAL 24 SEP 1996 - SEP 1998	
4. TITLE AND SUBTITLE DEVELOPMENT OF THE AERODYNAMIC/AEROSERVOELASTIC MODULES IN ASTROS / VOLUME III - AEROSERVOELASTICITY DISCIPLINE IN ASTROS APPLICATIONS MANUAL			5. FUNDING NUMBERS C: F33615-96-C-3217 PE: 65502F PR: STTR TA: 41 WU: 00	
6. AUTHOR(S) M. Karpel and B. Moulin Technion - I.I.T.				
7. PERFORMING ORGANIZATION NAME(S) AND ADDRESS(ES) Subcontractor to Research Insititute:      Prime Contractor: Technion - Israel Institute of Technology      ZONA Technology, Inc. Haifa 32000      7434 E. Stetson Drive, Suite 205 Israel      Scottsdale, AZ 85251 Tel 972-4-8293490 / Fax 972-4-8229352      Tel (602) 945-9988 / Fax (602) 945-6588			8. PERFORMING ORGANIZATION REPORT NUMBER  ZONA 99-11G	
9. SPONSORING/MONITORING AGENCY NAME(S) AND ADDRESS(ES) Air Vehicles Directorate Air Force Research Laboratory Air Force Materiel Command Wright Patterson Air Force Base OH 45433-7531 POC: Capt. Gerald Andersen, (937) 255-6992 / Dr. V.B.Venkayya (937) 255-2582			10. SPONSORING/MONITORING AGENCY REPORT NUMBER  AFRL-VA-WP-TR-2000-3042	
11. SUPPLEMENTARY NOTES				
12a. DISTRIBUTION AVAILABILITY STATEMENT  APPROVED FOR PUBLIC RELEASE; DISTRIBUTION UNLIMITED			12b. DISTRIBUTION CODE	
13. ABSTRACT (Maximum 200 words)  This Applications Manual presents two optimization cases of an advanced fighter aircraft (AFA) model demonstrating the capabilities of the aeroservoelastic module in ASTROS. The first case, presented in Part I, is an open-loop optimization case with flutter constraints. The second case, presented in Part II, is a closed-loop aeroservoelastic optimization case. Description of the input and output along with numerous plots are provided.  This report is part of the documentation which describe the complete development of an STTR Phase II effort entitled "Development of the Aerodynamic/Aeroservoelastic Modules in ASTROS". Additional aeroservoelasticity (ASE) reports are the Theoretical Manual, the User's Manual, and the Programmers Manual.				
14. SUBJECT TERMS  Multidisciplinary Optimization, Aeroelasticity, Aeroservoelasticity, Gust Response, ASTROS			15. NUMBER OF PAGES 36	
			16. PRICE CODE	
17. SECURITY CLASSIFICATION OF REPORT  UNCLASSIFIED	18. SECURITY CLASSIFICATION OF THIS PAGE  UNCLASSIFIED	19. SECURITY CLASSIFICATION OF ABSTRACT  UNCLASSIFIED	20. LIMITATION OF ABSTRACT  SAR	

## FOREWORD

This final report is submitted in fulfillment of CDRL CLIN 0001, Data Item A001, Title: Scientific and Technical Reports of a Small business Technology Transfer (STTR) Phase II contract No. F33615-96-C-3217 entitled, "Development of the Aerodynamic/Aeroservoelastic Modules in ASTROS," covering the performance period from 24 September 1996 to 24 September 1998.

This work is the second phase of a continuing two-phase STTR contract supported by AFRL/Wright-Patterson. The first phase STTR contract No. F33615-95-C-3219 entitled, "Enhancement of the Aeroservoelastic Capability in ASTROS," was completed in May 1996 and published as WL-TR-96-3119.

Both STTR Phase I and Phase II contracts are performed by the same ZONA Team in which ZONA Technology, Inc. is the prime contractor, whereby the team members include: the University of Oklahoma (OU), Universal Analytics, Inc. (UAI), and Technion (I.T.T.).

This final report consists of eight volumes, these are:

### ASTROS\*

- |            |   |                           |
|------------|---|---------------------------|
| Volume I   | - | ZAERO User's Manual       |
| Volume II  | - | ZAERO Programmer's Manual |
| Volume III | - | ZAERO Application Manual  |
| Volume IV  | - | ZAERO Theoretical Manual  |

### ASTROServo

- |            |   |  |
|------------|---|--|
| Volume I   | - | Aeroservoelastic Discipline in ASTROS, User's Manual       |
| Volume II  | - | Aeroservoelastic Discipline in ASTROS, Programmer's Manual |
| Volume III | - | Aeroservoelastic Discipline in ASTROS, Application Manual  |
| Volume IV  | - | Aeroservoelastic Discipline in ASTROS, Theoretical Manual  |

This document (Volume III) is the Application Manual of the Aeroservoelastic (ASE) interaction module developed to facilitate ASE analysis and the application of ASE stability and response constraints within ASTROS.

At AFRL/Wright-Patterson, Captain Gerald Andersen was the contract monitor and Dr. V. B. Venkayya was the initiator of the whole STTR effort. The technical advice and assistance received from Mr. Doug Niell of the MacNeal Schwendler Corporation, Dr. V. B. Venkayya and others from AFRL during the course of the present phase on the development of ASTROS\* are gratefully acknowledged.

## TABLE OF CONTENTS

	Page
<b>PART I: OPTIMIZATION OF A FIGHTER AIRCRAFT WITH FLUTTER CONSTRAINTS USING ASTROZ</b>	
1. Introduction .....	1
2. Structural and Aerodynamic Models .....	1
3. Normal Modes Analysis .....	1
4. Minimum-State Aerodynamic Approximations .....	1
5. Flutter Constraints .....	2
6. Baseline Analyses and Sensitivities .....	2
7. General Results of Optimizations .....	3
7.1 Optimization with 8 modes .....	3
7.2 Optimization with 13 modes .....	3
Tables for Part I .....	4
Figures for Part I .....	5
 <b>PART II: ASE OPTIMIZATION OF A FIGHTER AIRCRAFT USING ASTROZ</b>	
1. Introduction .....	27
2. Structural and Aerodynamic Models .....	27
3. Control System .....	27
4. Flutter Constraints .....	28
5. Control Constraints .....	28
6. Stress Constraints .....	28
7. General Results of Optimizations .....	28
7.1 Case 1: High aeroelastic gain requirement .....	28
7.2 Case 2: Moderate aeroelastic gain requirement .....	29
Figures for Part II .....	30

## LIST OF FIGURES

<b>PART I:</b>	<b>Page</b>
Figure 1. AFA structural model .....	5
Figure 2. AFA wing structural model .....	5
Figure 3. Unsteady aerodynamic model .....	6
Figure 4. Grid points splined to aerodynamic model .....	6
Figure 5. Grid points of the a-set .....	7
Figure 6. Normal mode shapes for the structural and aerodynamic models. Frequencies 0.0 Hz (lift); 0.0 Hz (pitch); 3.628 Hz .....	8
Figure 7. Normal mode shapes for the structural and aerodynamic models. Frequencies 5.516 Hz; 10.679 Hz; 14.474 Hz .....	9
Figure 8. Normal mode shapes for the structural and aerodynamic models. Frequencies 15.510 Hz; 21.132 Hz; 22.962 Hz .....	10
Figure 9. Normal mode shapes for the structural and aerodynamic models. Frequencies 28.162 Hz; 29.763 Hz; 37.947 Hz .....	11
Figure 10. MIST approximation with 10 modes (left plots – with constraints; right plots - without constraints) .....	12
Figure 11. MIST approximation with 10 modes (left plots – with constraints; right plots - without constraints) .....	13
Figure 12. MIST approximation with 12 modes (8 lags) (left plots – with constraints; right plots - without constraints) .....	14
Figure 13. MIST approximation with 12 modes (8 lags) (left plots – with constraints; right plots - without constraints) .....	15
Figure 14. MIST approximation with 12 modes (10 lags) (left plots – with constraints; right plots - without constraints) .....	16
Figure 15. MIST approximation with 12 modes (10 lags) (left plots – with constraints; right plots - without constraints) .....	17

## LIST OF FIGURES (continued)

	Page
Figure 16. ASTROS and ASE with MIST approximation (10 modes; upper plot – with constraints; lower plot - without constraints) .....	18
Figure 17. ASTROS and ASE with MIST approximation (12 modes, 8 lags; upper plot - with constraints; lower plot - without constraints) .....	19
Figure 18. ASTROS and ASE with MIST approximation (12 modes, 10 lags; upper plot - with constraints; lower plot – without constraints) .....	20
Figure 19. Baseline flutter analysis .....	21
Figure 20. Baseline sensitivities of the flutter constraints .....	22
Figure 21. Baseline sensitivities of the flutter constraints .....	23
Figure 22. Baseline sensitivities of the flutter constraints .....	24
Figure 23. Optimization weight history (first iterations) .....	25
Figure 24. Optimization weight history (13 modes) .....	25
Figure 25. ASE flutter analysis (13 modes) .....	26
Figure 26. ASE flutter analysis (13 modes) .....	26

## LIST OF FIGURES (continued)

	Page
<b>PART II:</b>	
Figure 27. AFA structural model – different view .....	30
Figure 28. Control system interconnection model for the numerical example .....	30
Figure 29. ASE optimization weight history (Case 1) .....	31
Figure 30. Root loci for the baseline and final design structures (Case 1) .....	31
Figure 31. Aeroelastic system gain history (Case 1) .....	32
Figure 32. Positive gain margin history (Case 1) .....	32
Figure 33. Positive phase margin history (Case 1) .....	33
Figure 34. Histories of controller gain factors (Case 1) .....	33
Figure 35. ASE optimization weight history (Case 2) .....	34
Figure 36. Root loci for the baseline and final design structures (Case 2) .....	34
Figure 37. Aeroelastic system gain history (Case 2) .....	35
Figure 38. Positive gain margin history (Case 2) .....	35
Figure 39. Positive phase margin history (Case 2) .....	36
Figure 40. Histories of controller gain factors (Case 1) .....	36



## LIST OF TABLES

	Page
Table 1. Final weighted error for MIST approximation .....	4
Table 2. Flutter dynamic pressure [psi] for MIST approximation .....	4
Table 3. Flutter frequency [rad/s] for MIST approximation .....	4

# **PART I: OPTIMIZATION OF A FIGHTER AIRCRAFT WITH FLUTTER CONSTRAINTS USING ASTROZ**

## **1. Introduction**

This document contains the results of an optimization with flutter constraints using ASTROZ (ASTROS with the new ZAERO aerodynamics) and the new aeroservoelasticity (ASE) discipline. The application is to an advanced fighter aircraft (AFA) model. The results are shown in comparison with the existing flutter discipline in ASTROS Version 11.

## **2. Structural and Aerodynamic Models**

A top view of the aircraft structural model is shown in Figure 1. The wing is made of aluminum. The subject for structural optimization was the skin of the wing torsion box. A top view of the wing box divided into 13 design zones is shown in Figure 2. Initial design thicknesses of the wing upper skin were set to 2.0 *inches* for zones 1 - 3, to 1.5 *inches* for zones 4 - 9, and to 1.0 *inch* for zones 10 - 13. Those for the lower skin thicknesses were set to 2.0 *inches* for zones 1 - 6 and to 1.0 *inch* for zones 7 - 13.

The unsteady aerodynamic model is shown in Figure 3. The model consisted of 9 aerodynamic panels representing the fuselage, the inboard and outboard sections of the wing, the four control surfaces, the tip missile, and the horizontal tail. The panels representing the fuselage and the horizontal tail were attached to the support grid point of the structural model. Four root boxes of the inboard LEF panel were also attached to this point. The wing, the control surfaces, and the missile panels were splined to the grid points as shown in Figure 4.

## **3. Normal Modes Analysis**

Normal modes analysis was carried out for symmetric boundary conditions with two rigid-body degrees of freedom (plunge and pitch). Guyan static condensation was applied to the 135 grid points of Figure 5 included in the retained (a-set) coordinates. The a-set coordinates were in  $z$  direction at all of the 135 points, in  $x$  direction at the leading edge of the wing and at one point in the missile, and in  $\theta_x$  at the supported point (marked by \* in Figure 5).

The first 12 natural modes are shown in Figures 6-9. The shapes on the left are based on modal displacements at the structural points, and those on the right side at the aerodynamic boxes.

## **4. Minimum-State Aerodynamic Approximations**

The Minimum-State (MS) approximation with physical weighting was applied to the AFA model with ZAERO aerodynamics. Parameters for the physical weighting were  $NWD = 3$ ,  $WCUT = 0.1$ , and  $PDAMP = 0.1$  (see the PWEIGHT entry in the User's Manual for details). The numbers of lag terms were 8 and 10. Approximation root values were calculated by the default equation

$$R_i = -1.7k_{\max} \left( \frac{i}{n_i + 1} \right), \quad i=1, n_i$$

where  $k_{\max}$  is the maximum reduced frequency of the aerodynamic data and  $n_i$  is the number of approximation roots.

Two cases were considered: 10 modes in flutter analysis and 12 modes. In the first case, 13  $k$  values were used: 0.0001, 0.01, 0.02, 0.03, 0.04, 0.045, 0.05, 0.055, 0.065, 0.08, 0.12, 0.18, and 0.27. In the second case, 14  $k$  values were used, with the  $k$  value of 0.27 replaced by the  $k$  values of 0.24 and 0.3.

Final weighted errors for the MIST approximation with different numbers of modes and lags are given in Table 1. The "constraint" case required a perfect fit at  $k = 0$  and  $k = k_{\max}$ . Fitting for some terms is shown in Figures 10 and 11 for the 10 modes / 8 lags case, in Figures 12 and 13 for the 12 modes / 8 lags case, and in Figures 14 and 15 for the 12 modes / 10 lags case. The flutter dynamic pressures obtained for the three approximation cases are compared with those of the standard ASTROZ code in Table 2. Flutter frequencies are shown in Table 3. Root loci for the approximation cases are shown in Figures 16 -18.

## 5. Flutter Constraints

Flutter optimization was performed for symmetric boundary conditions at Mach number 0.9. Ten modes, including two rigid-body modes were used to account for the structural changes during the optimization. The two rigid-body modes were omitted in the flutter analyses, however, because the standard P-K routine of ASTROS has problems with rigid-body modes. Fourteen reduced frequency values were used to create the aerodynamic database: 0.0001, 0.01, 0.02, 0.03, 0.04, 0.045, 0.05, 0.055, 0.065, 0.08, 0.12, 0.18, 0.24, and 0.30. Flutter design points were defined at fifteen velocity values in *inches/sec* at sea level: 10000.0, 11000.0, 12000.0, 13000.0, 14000.0, 15000.0, 16000.0, 17000.0, 18000.0, 19000.0, 20000.0, 21000.0, 22000.0, 23000.0, and 24000.0. The flutter constraints required the damping to be positive at all of the design points.

## 6. Baseline Analyses and Sensitivities

State-space flutter analyses were performed using the MS approximation with 10 lags as described in Section 4. The root loci for the baseline flutter analyses using the P-K and ASE methods are shown in Figure 19. It can be observed that the agreement between the two methods is good, and that the flutter velocities in both cases are slightly less than 22000 *in/sec*, which violates the flutter constraints. Sensitivities of the most critical flutter constraints to the design variables are given in Figures 20 - 22.

## 7. General Results of Optimizations

### 7.1 Optimization with 8 modes

Five optimization runs were compared between the P-K method and the ASE method with  $n_{UP} = 1$ ,  $n_{UP} = 3$ ,  $n_{UP} = 4$ , and  $n_{UP} = 5$ . Note that  $n_{UP} = 1$  means the modal database is updated at every iteration. The move limit was set to 1.3.

Optimization histories are given in Figure 23. The results of the P-K and ASE optimizations with  $n_{UP}$  equal to 1 and 3 are very close. For  $n_{UP}$  larger than 3, there was a jump in the third iteration but afterwards the ASE results moved closer to the P-K ones once again. This shows that updating the modal database after the third iteration is important because of the considerable changes in the structure (the designed weight was decreased by approximately 60 %).

Detailed investigation shows that, in the 9-th iteration of the optimization process, the last high frequency mode used in the flutter analysis was replaced by another one because of the modification of the structure. This switch in the high frequency modes from iteration to iteration caused divergence of the design procedure. To avoid this phenomenon, more modes should be used in the optimization process. This new case will be described below.

### 7.2 Optimization with 13 modes

The optimization process was repeated with the same baseline structure, but with 13 elastic modes taken into account. Constraints were assigned at 13 velocity values in *inches/sec*: 10000.0, 11000.0, 12000.0, 13000.0, 14000.0, 15000.0, 16000.0, 17000.0, 18000.0, 19000.0, 20000.0, 21000.0, and 22000.0. The damping parameter  $g(\omega_h)$  was set to 0.02 for all frequencies. Because of numerical problems, the P-K method was not applied.

The optimization history is shown in Figure 24. There was no convergence in 15 iterations, but the design after the 10-th iteration did not violate the constraints. The root loci for the baseline and final iteration are shown in Figure 25. The root loci for the baseline and the 10-th iteration are shown in Figure 26. We can observe that, at the 10-th iteration, the design does not flutter and can be considered as successful.

An optimization using the P-K method did not give relevant results in this case because of numerical problems. The eigenvalues of the high frequency modes, which have considerable damping (Figure 25), did not seem to be calculated correctly and gave erroneous indications of flutter.

## TABLES FOR PART I

**Table 1. Final weighted error for MIST approximation**

Number of Modes/Lags	Final Error	
	Constraints	No Constraints
10/8	0.16923	0.15016
12/8	0.25390	0.22744
12/10	0.20286	0.17033

**Table 2. Flutter dynamic pressure [psi] for MIST approximation**

Number of Modes/Lags	ASTROZ Standard Flutter	ASTROZ with ASE			
		Constraints		No Constraints	
		Value	Error, %	Value	Error, %
10/8	18.701	18.550	-0.8	19.227	2.8
12/8	18.846	20.782	10.2	19.435	3.1
12/10	18.846	19.682	4.4	18.904	0.3

**Table 3. Flutter frequency [rad/s] for MIST approximation**

Number of Modes/Lags	ASTROZ Standard Flutter	ASTROZ with ASE			
		Constraints		No Constraints	
		Value	Error, %	Value	Error, %
10/8	46.648	46.840	0.4	47.311	1.4
12/8	46.801	48.540	3.7	47.797	2.1
12/10	46.801	47.922	2.4	47.027	0.5

## FIGURES FOR PART I

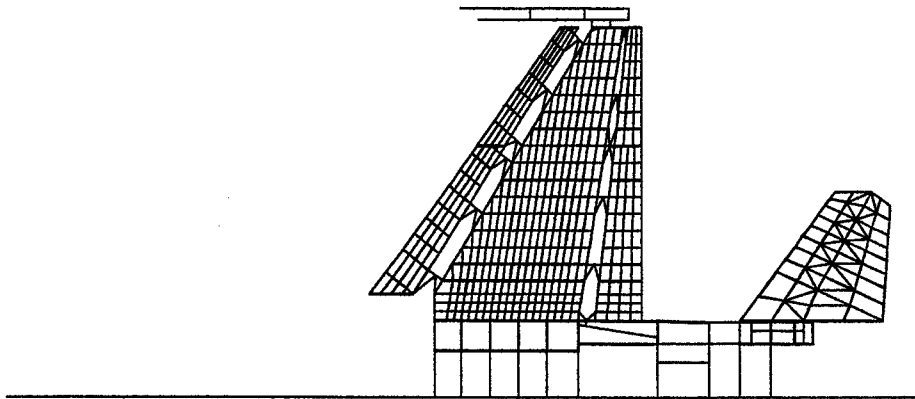


Figure 1. AFA structural model.

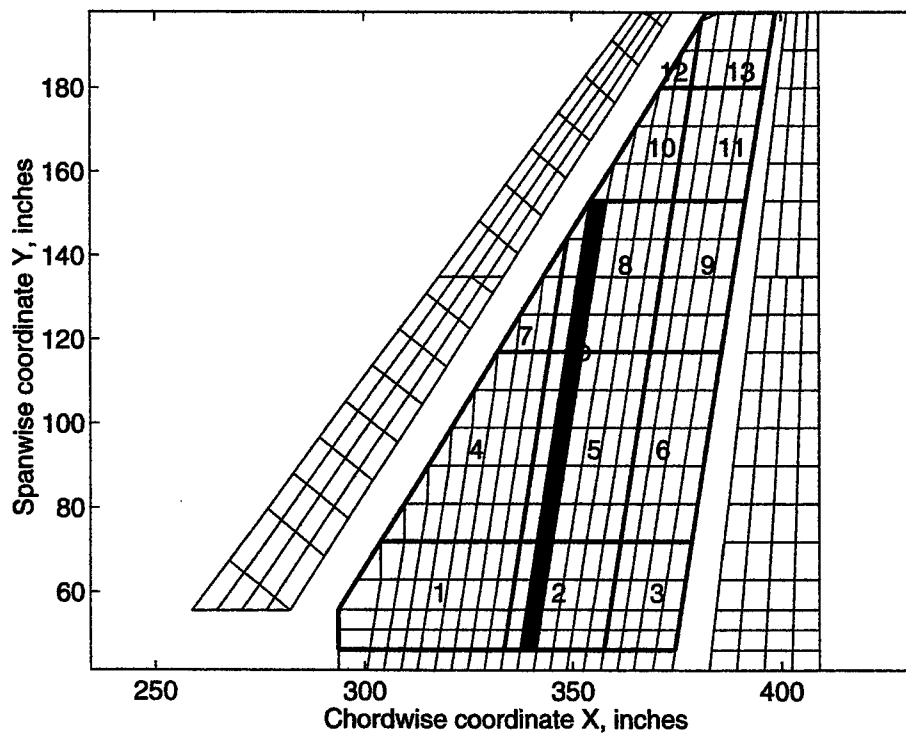
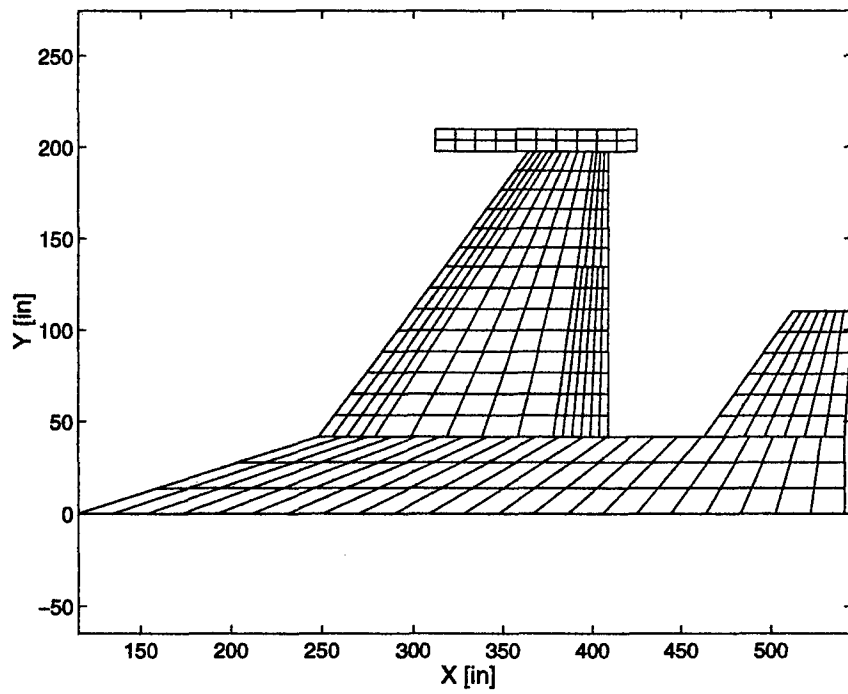
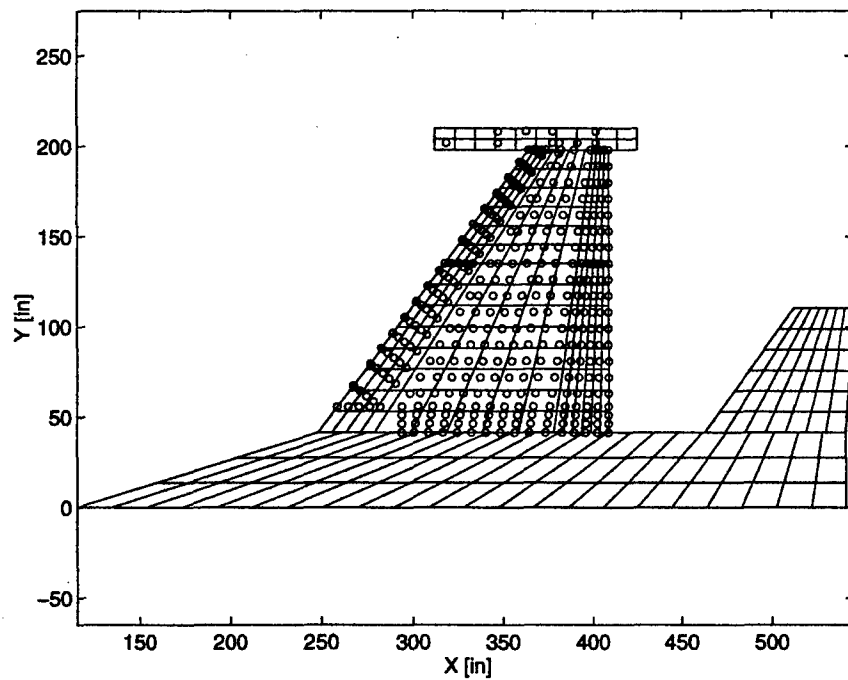


Figure 2. AFA wing structural model.



**Figure 3. Unsteady aerodynamic model.**



**Figure 4. Grid points splined to aerodynamic model.**

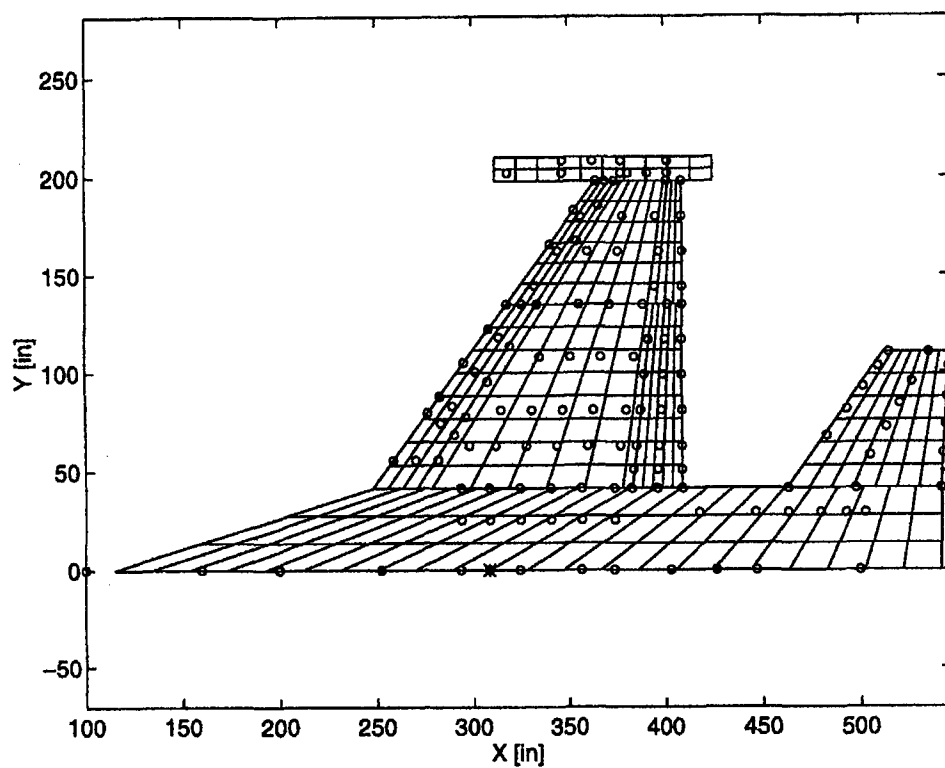
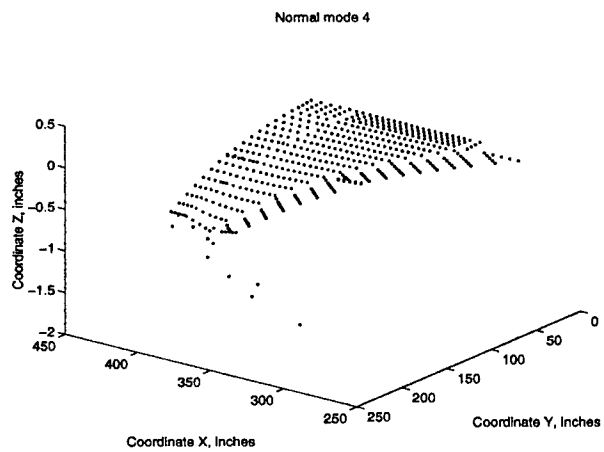
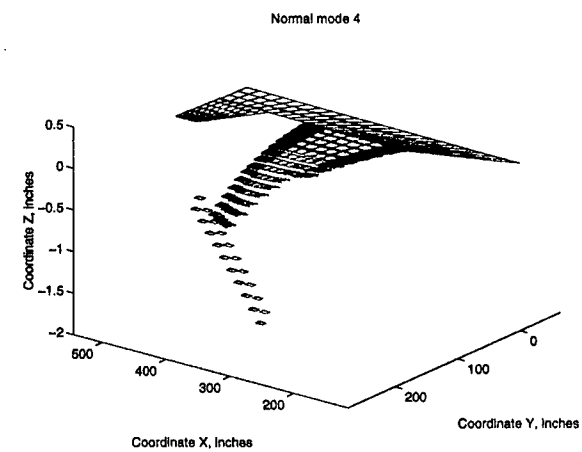
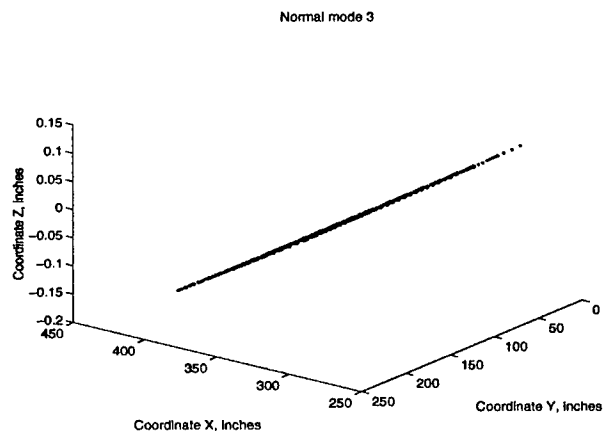
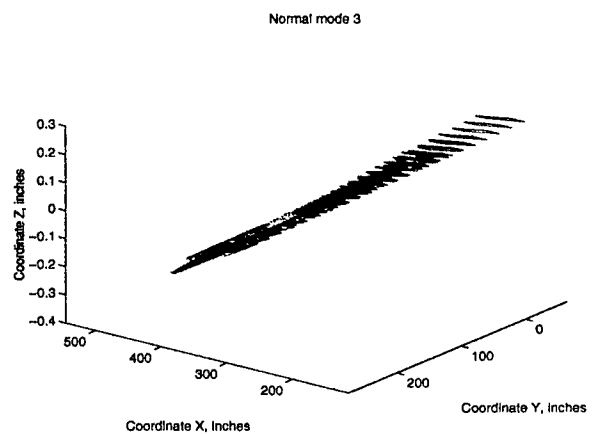
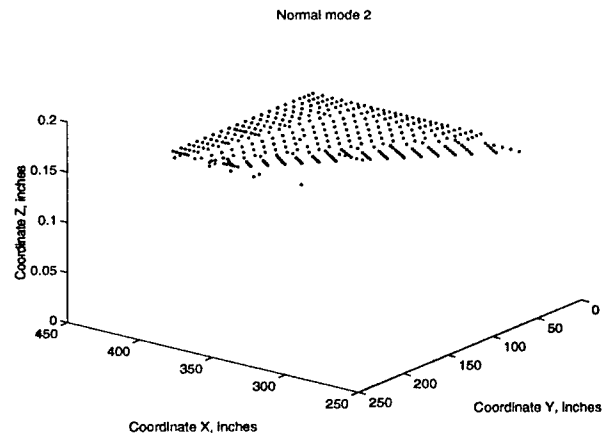
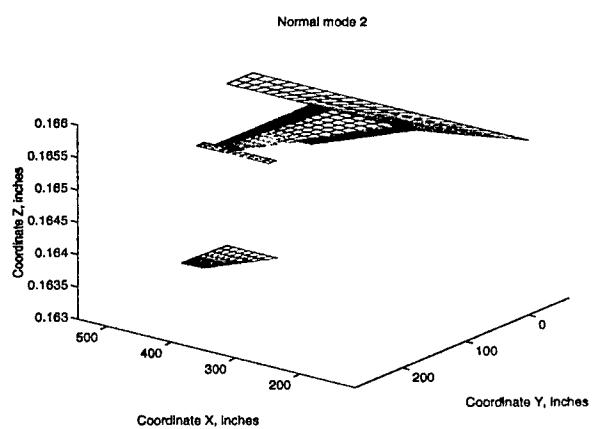


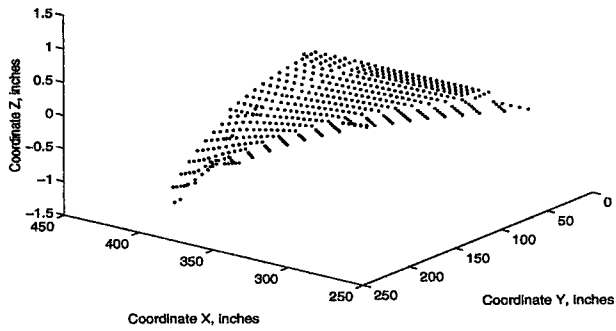
Figure 5. Grid points of the a-set.



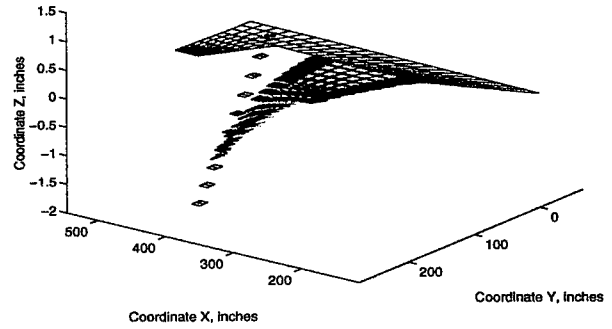


**Figure 6. Normal mode shapes for the structural and aerodynamic models.  
Frequencies 0.0 Hz (lift); 0.0 Hz (pitch); 3.628 Hz.**

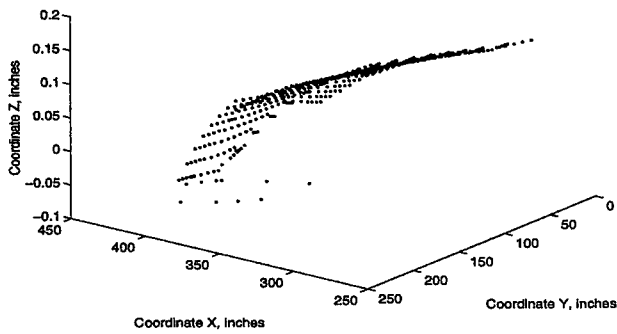
Normal mode 5



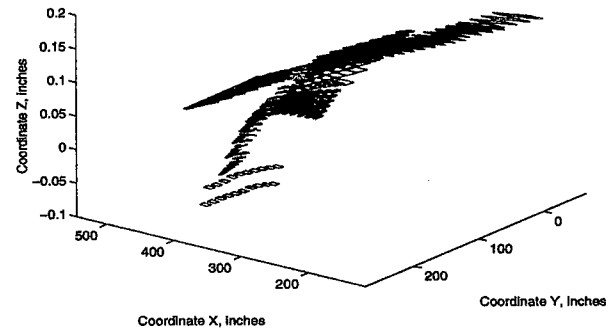
Normal mode 5



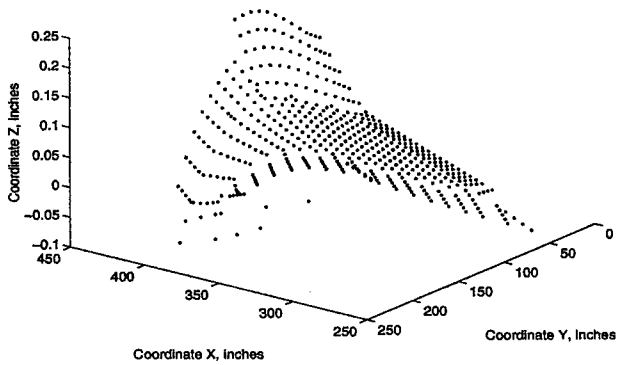
Normal mode 6



Normal mode 6



Normal mode 7



Normal mode 7

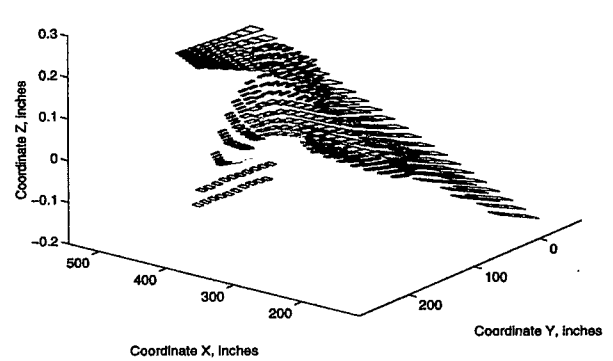


**Figure 7. Normal mode shapes for the structural and aerodynamic models.  
Frequencies 5.516 Hz; 10.679 Hz; 14.474 Hz.**

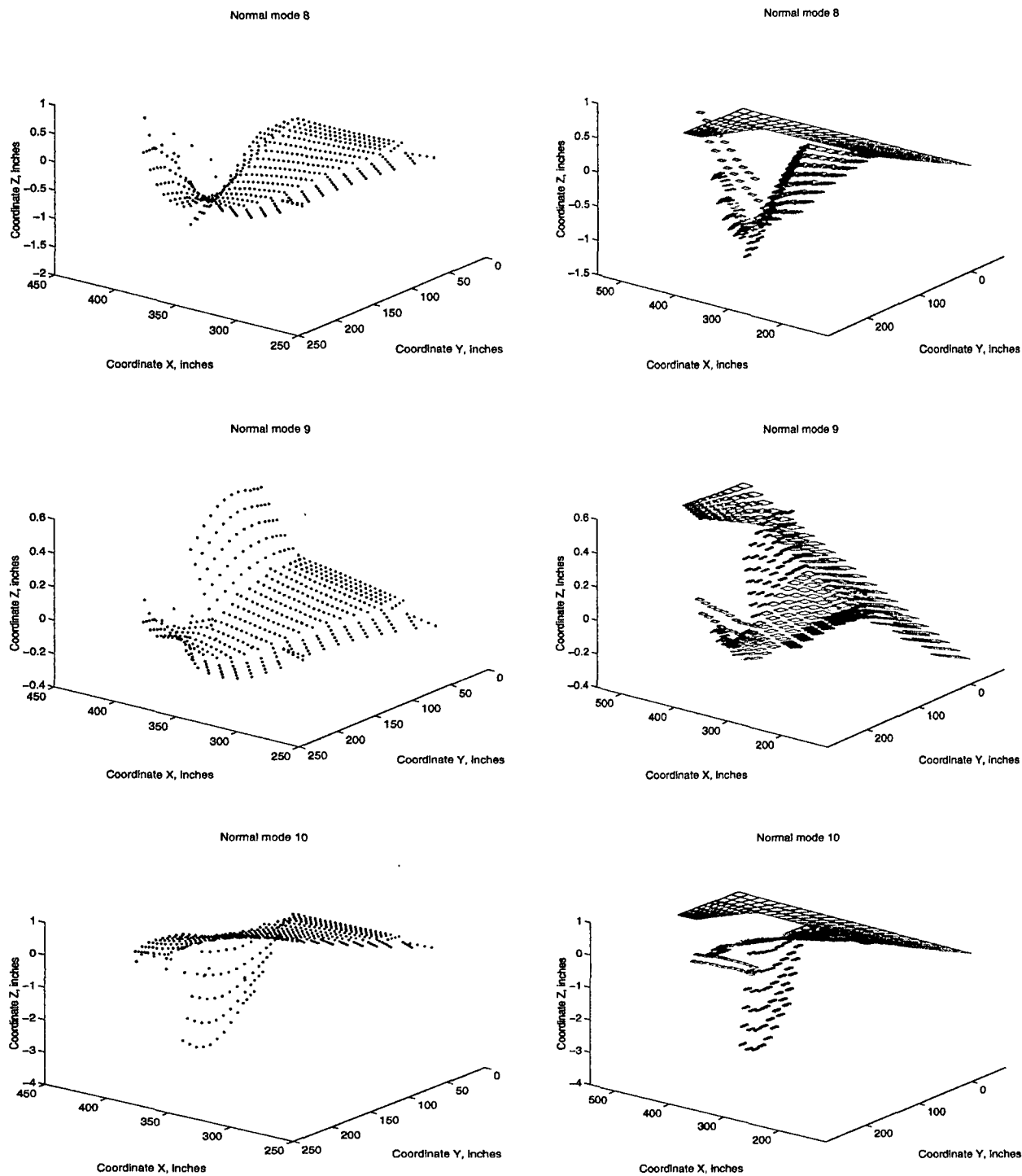
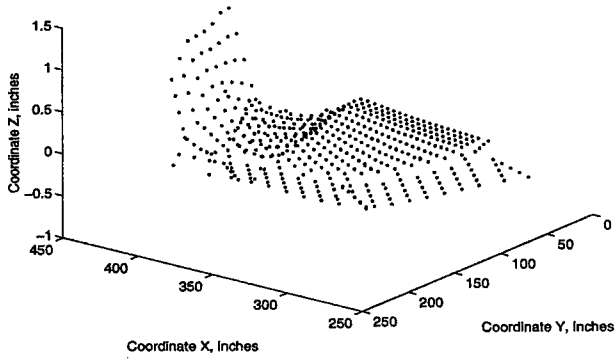
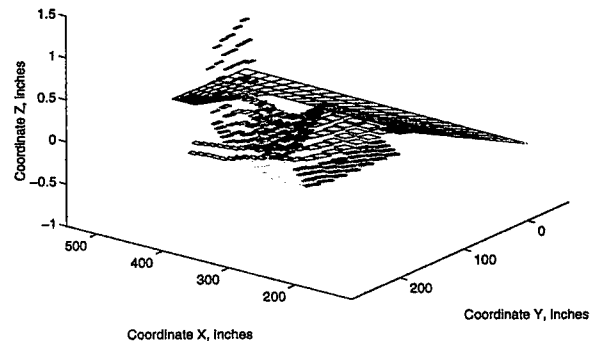


**Figure 8. Normal mode shapes for the structural and aerodynamic models.  
Frequencies 15.510 Hz; 21.132 Hz; 22.962 Hz.**

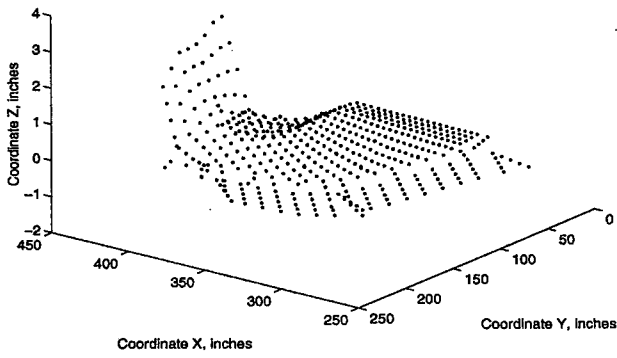
Normal mode 11



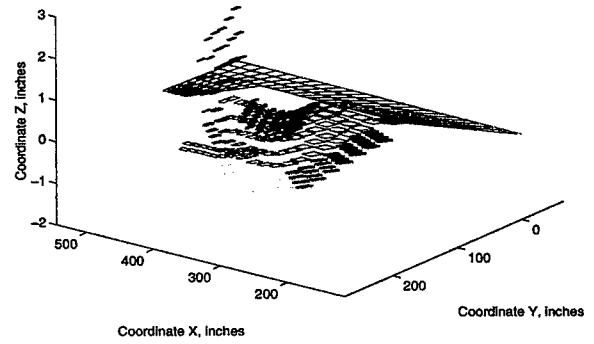
Normal mode 11



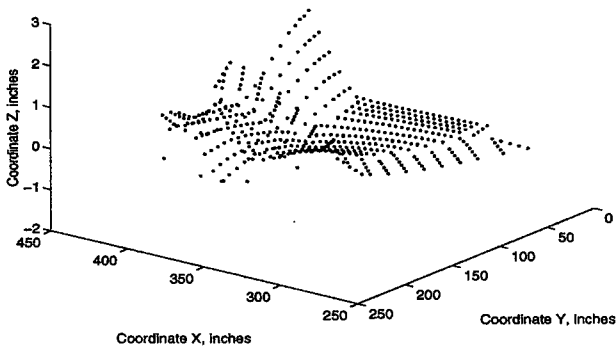
Normal mode 12



Normal mode 12



Normal mode 13



Normal mode 13

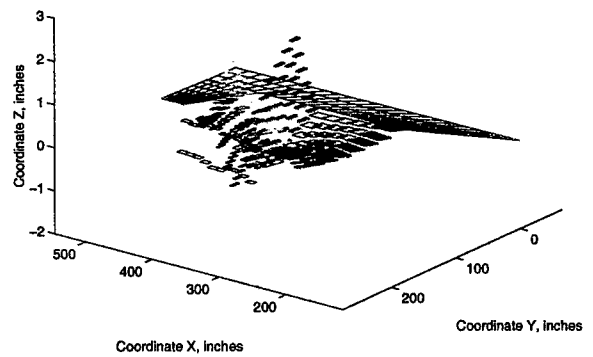


**Figure 9. Normal mode shapes for the structural and aerodynamic models.  
Frequencies 28.162 Hz; 29.763 Hz; 37.947 Hz.**

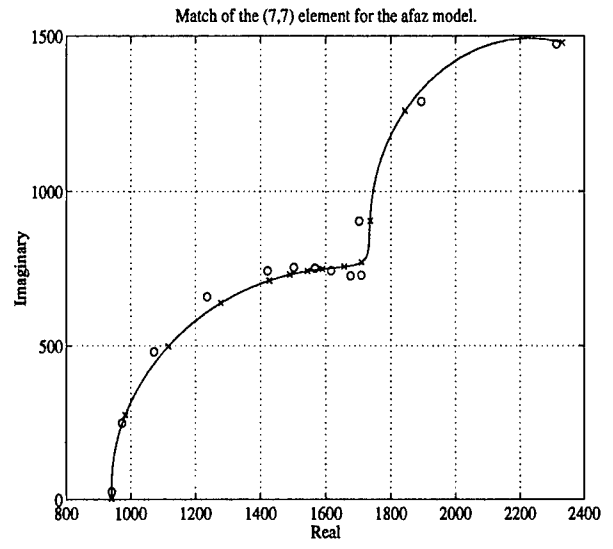
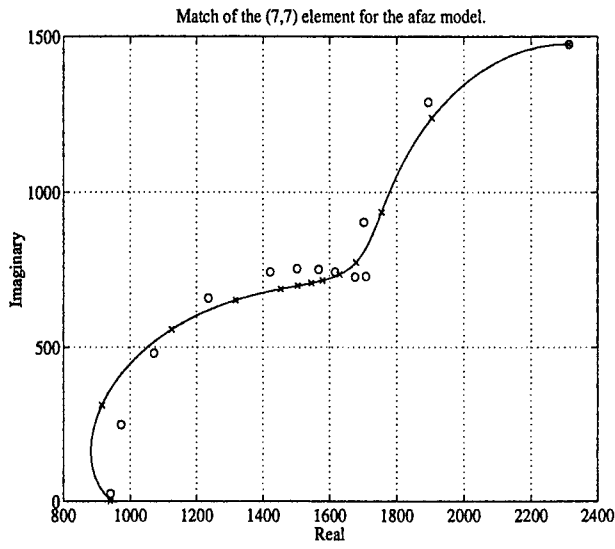
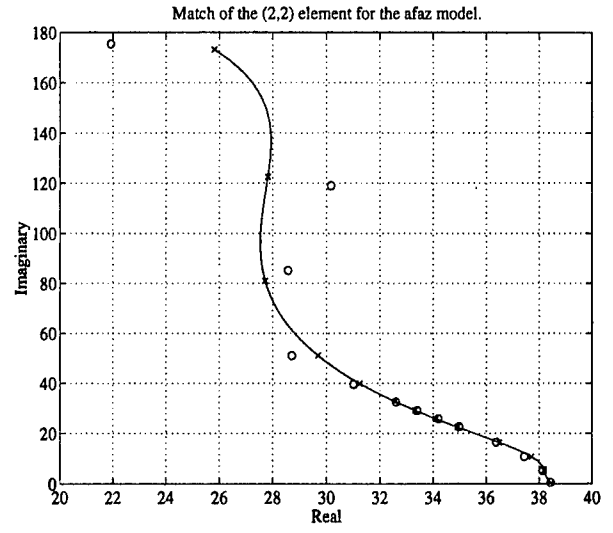
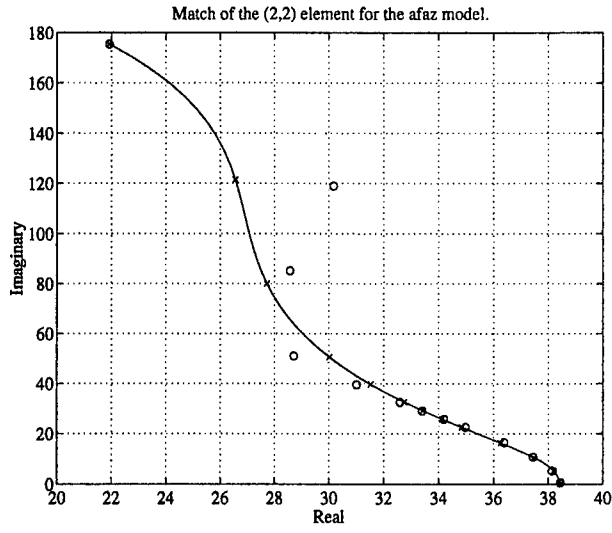


**Figure 10. MIST approximation with 10 modes (left plots – with constraints; right plots – without constraints).**

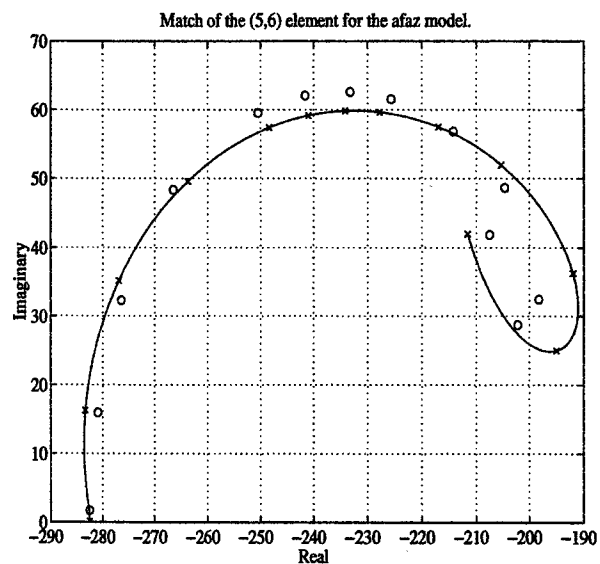
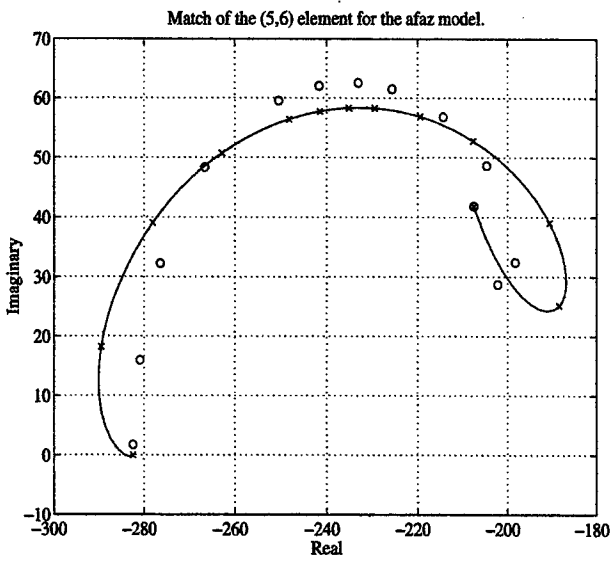
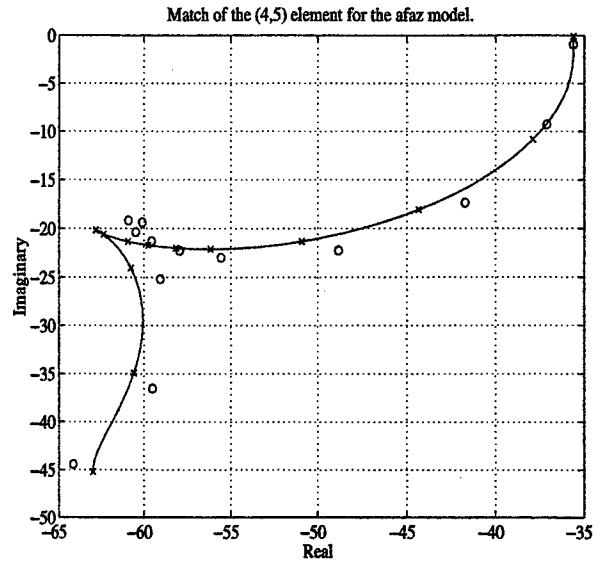
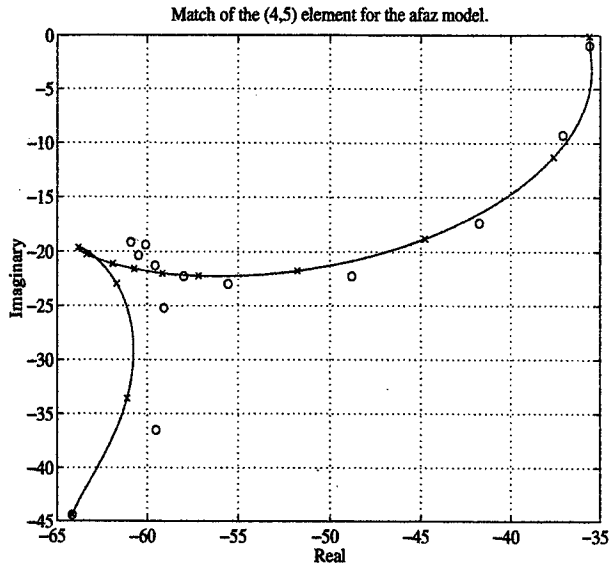


**Figure 11. MIST approximation with 10 modes (left plots - with constraints; right plots - without constraints).**

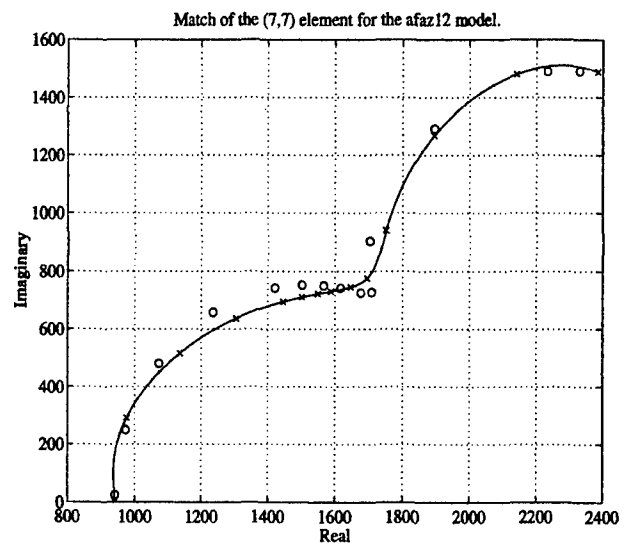
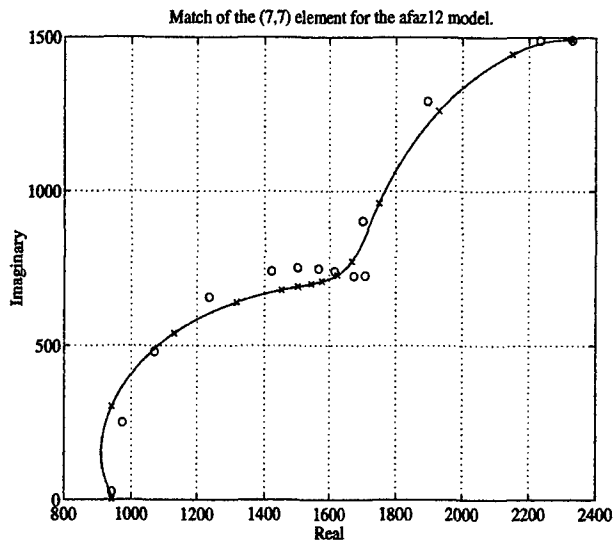
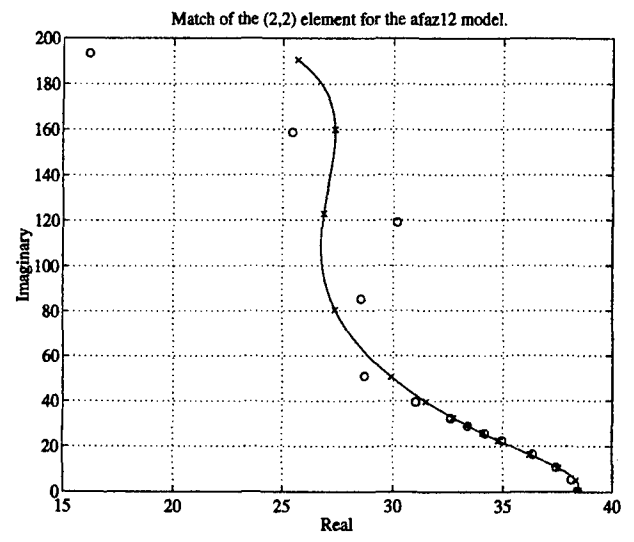
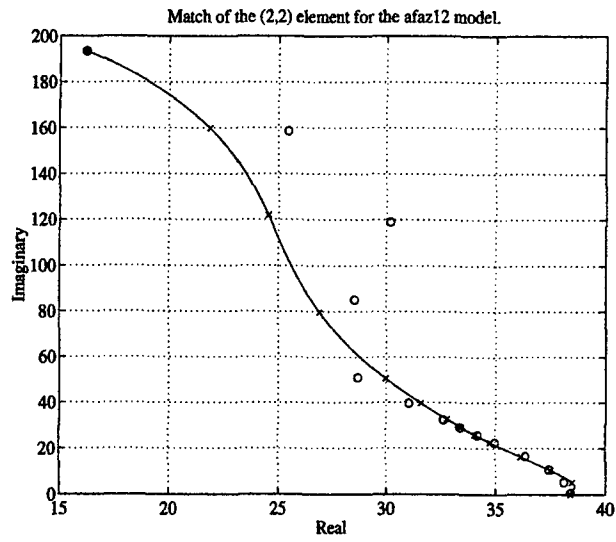


**Figure 12. MIST approximation with 12 modes (8 lags) (left plots - with constraints; right plots - without constraints).**

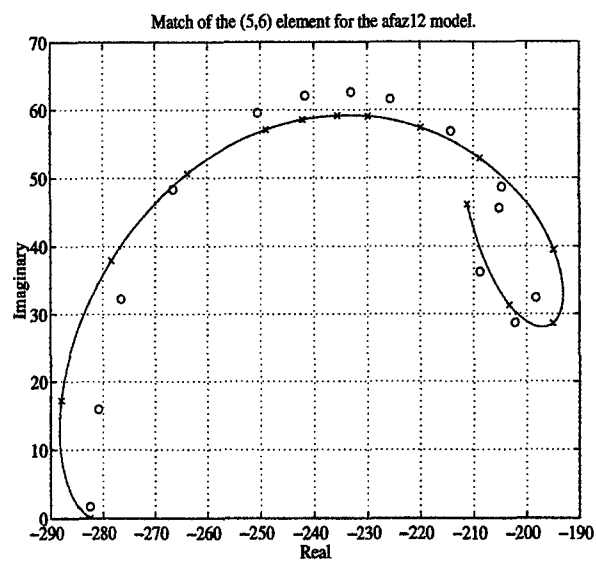
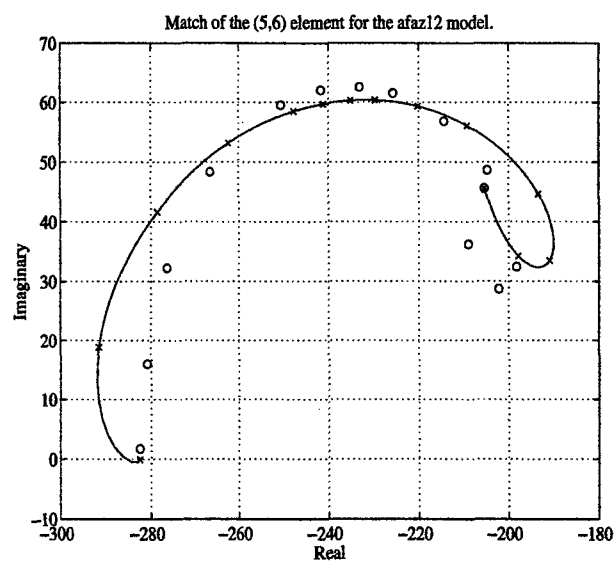
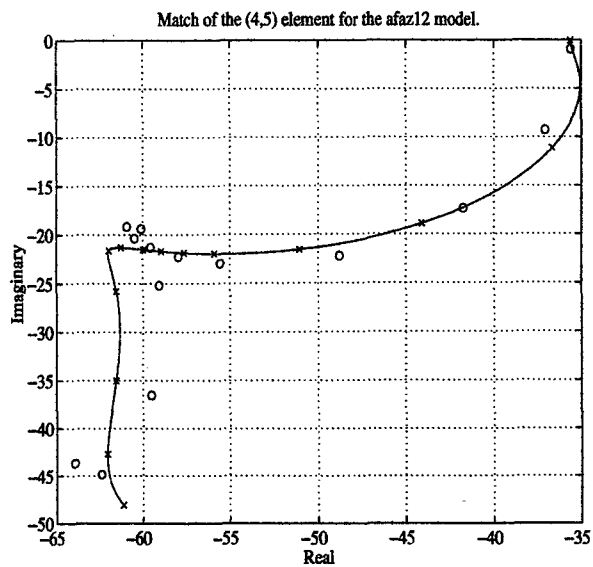
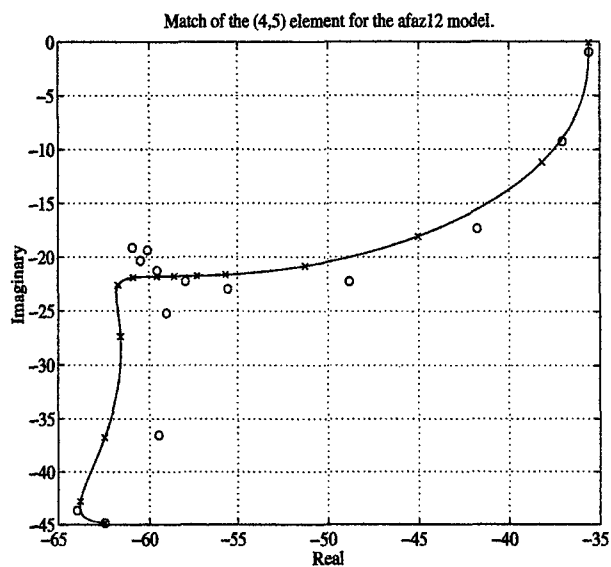


**Figure 13. MIST approximation with 12 modes (8 lags) (left plots - with constraints; right plots - without constraints).**



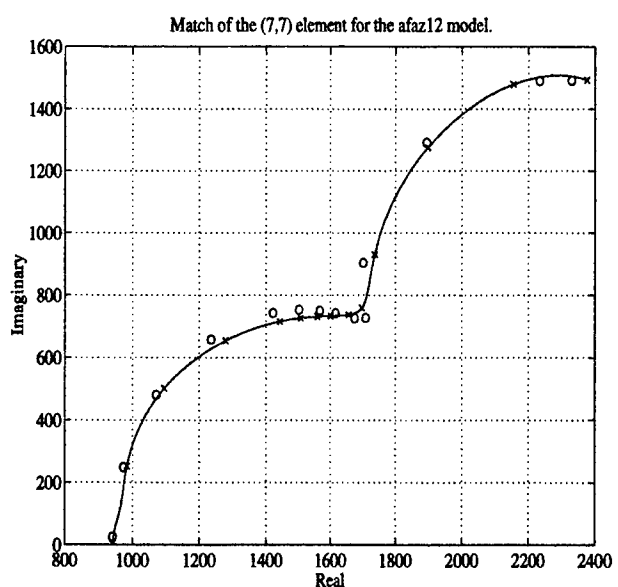
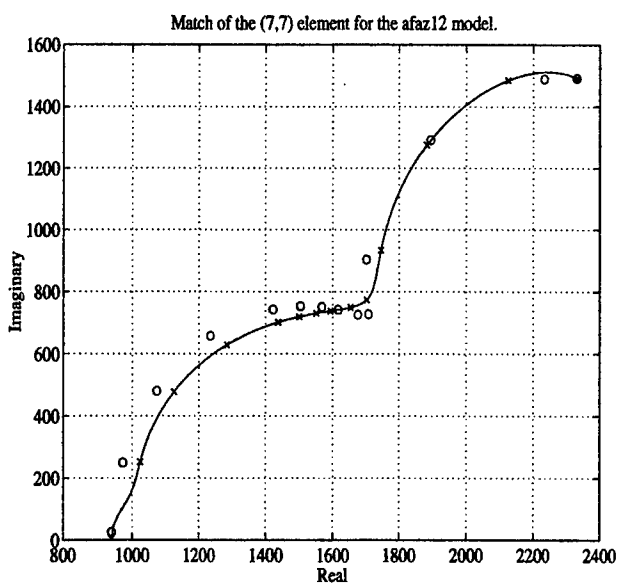
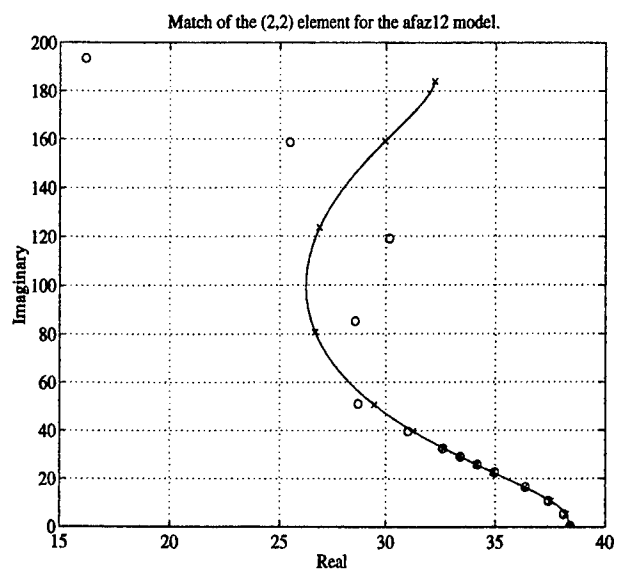
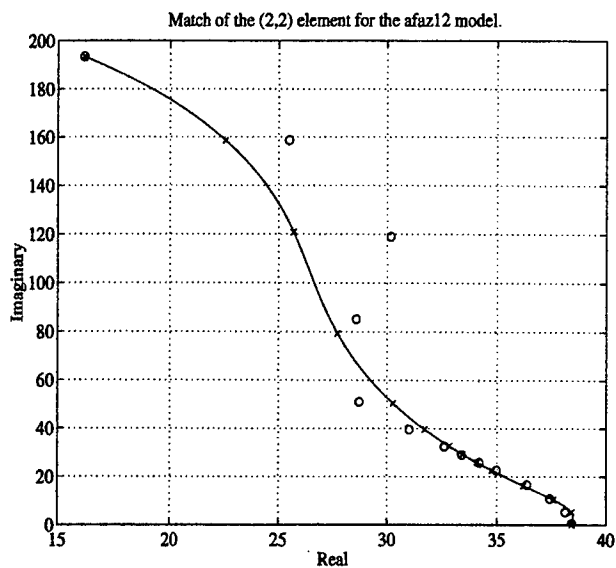


**Figure 14. MIST approximation with 12 modes (10 lags) (left plots - with constraints; right plots - without constraints)**

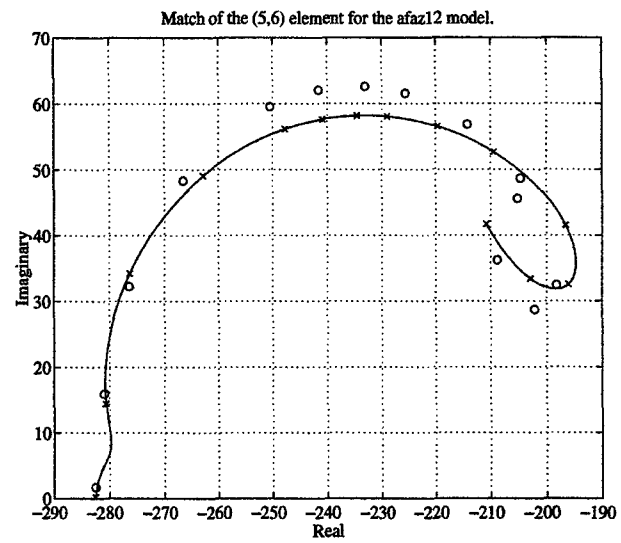
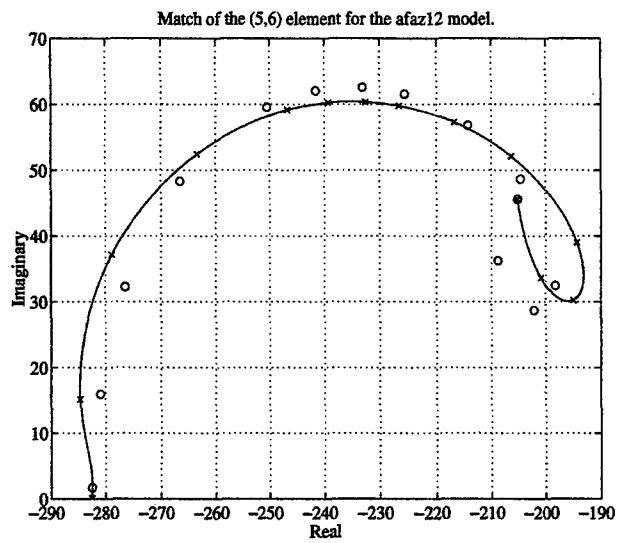
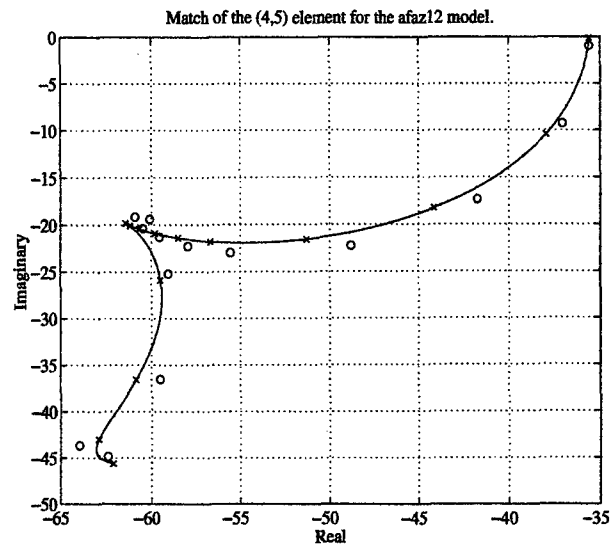
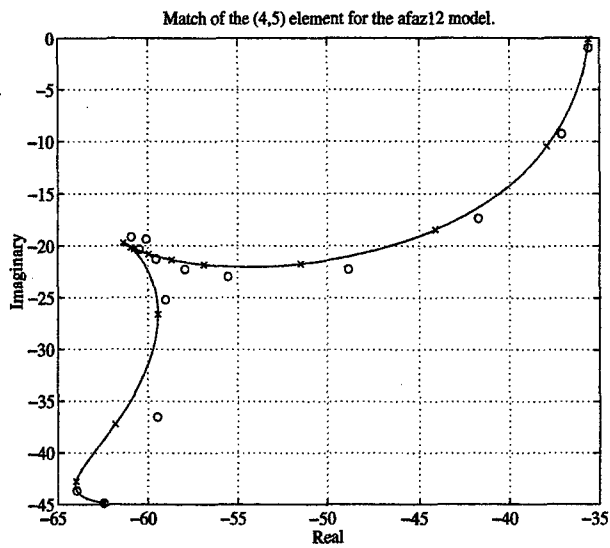


**Figure 15. MIST approximation with 12 modes (10 lags) (left plots – with constraints; right plots - without constraints).**

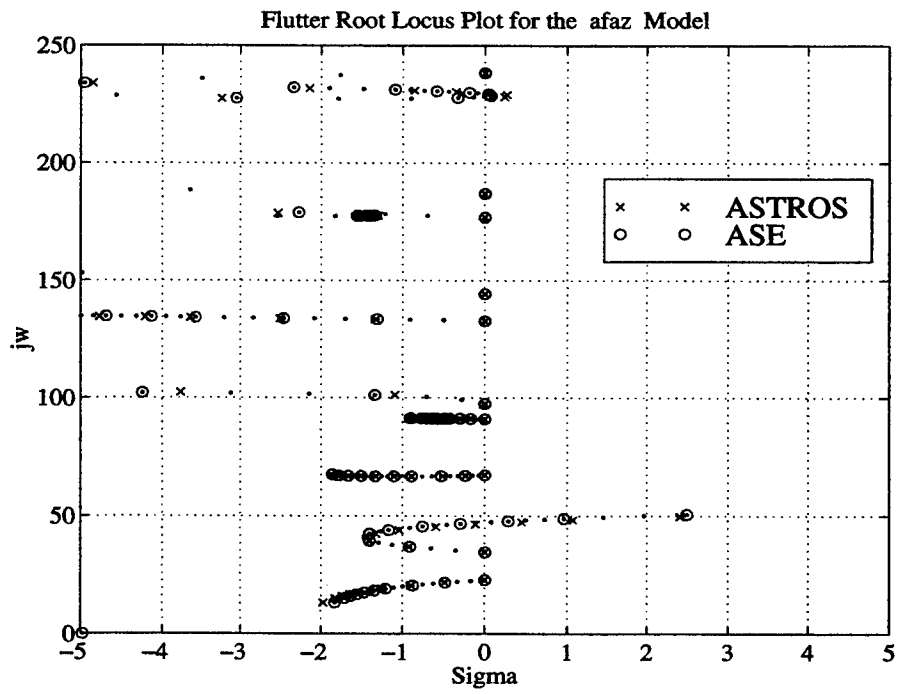
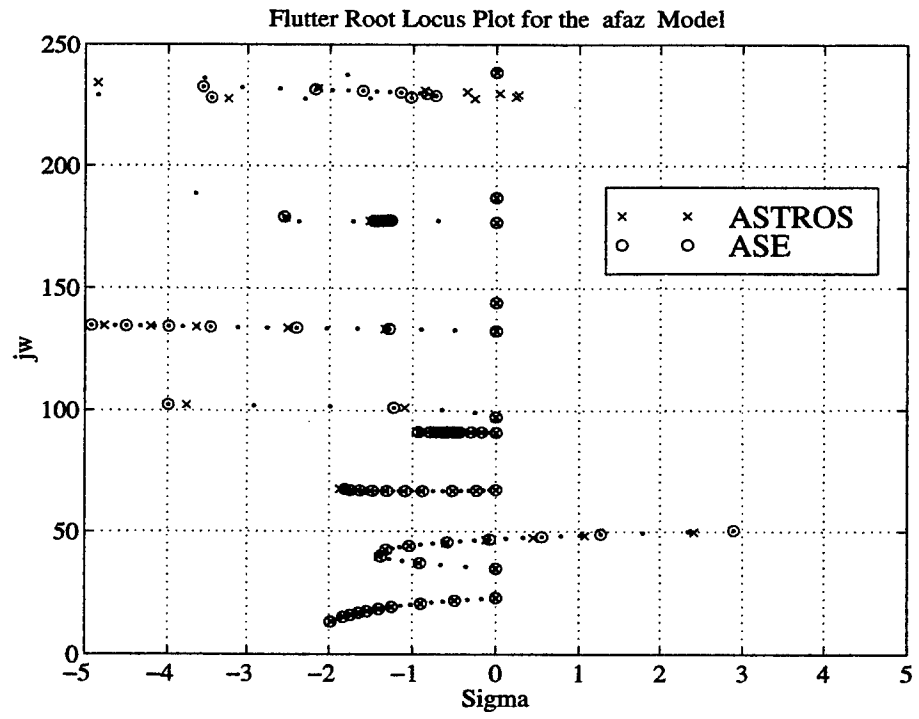


**Figure 16. ASTROS and ASE with MIST approximation (10 modes; upper plot - with constraints; lower plot - without constraints).**

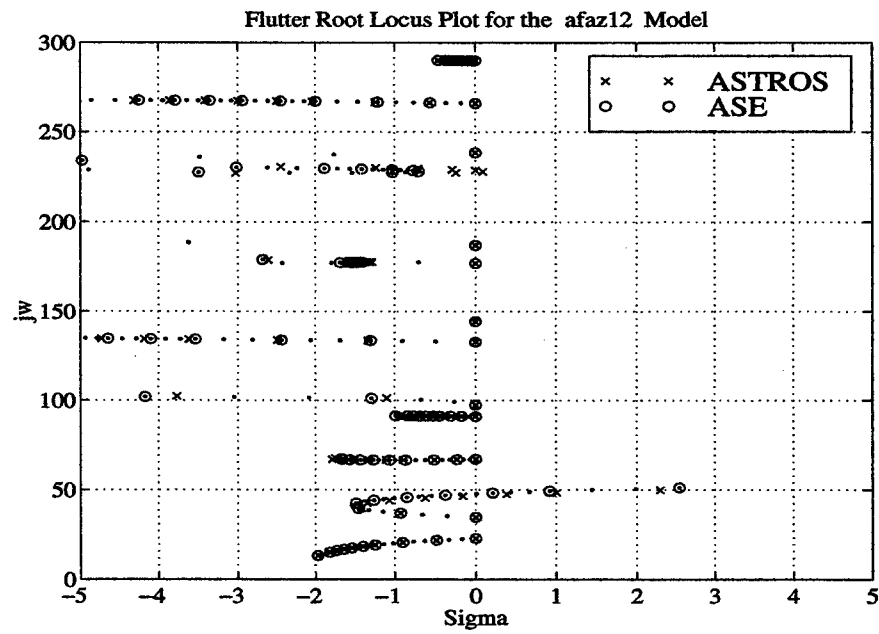
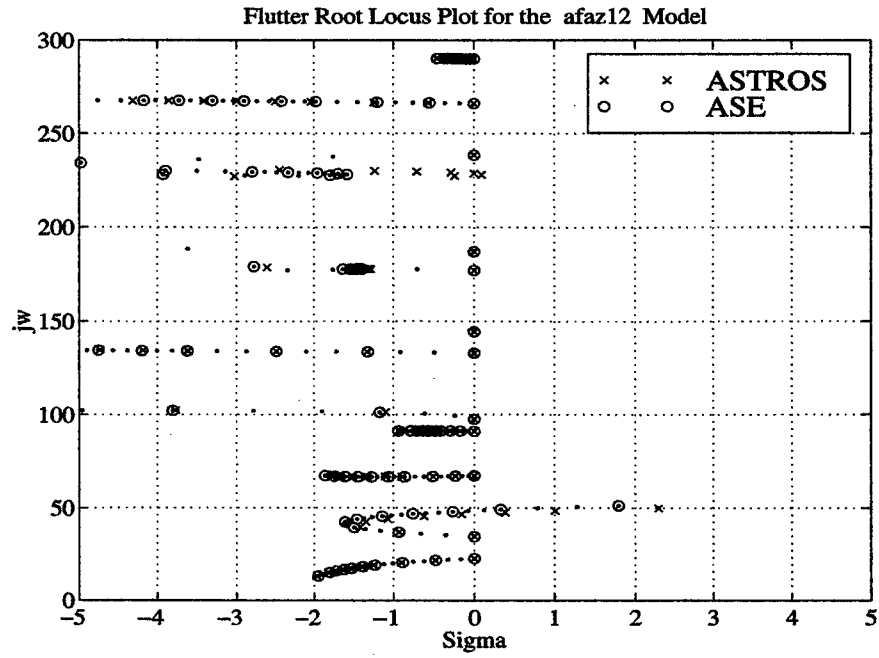


**Figure 17. ASTROS and ASE with MIST approximation (12 modes, 8 lags; upper plot - with constraints; lower plot - without constraints).**

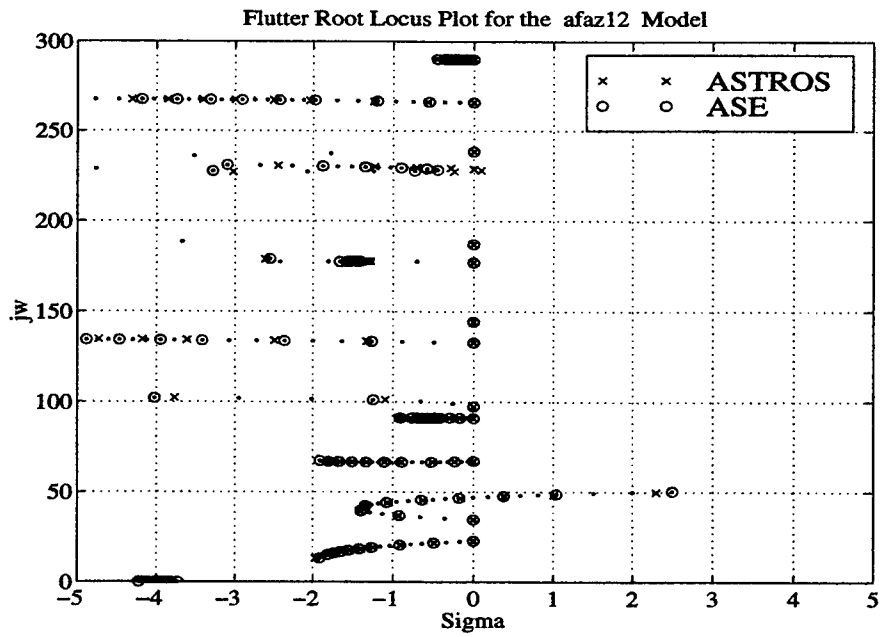
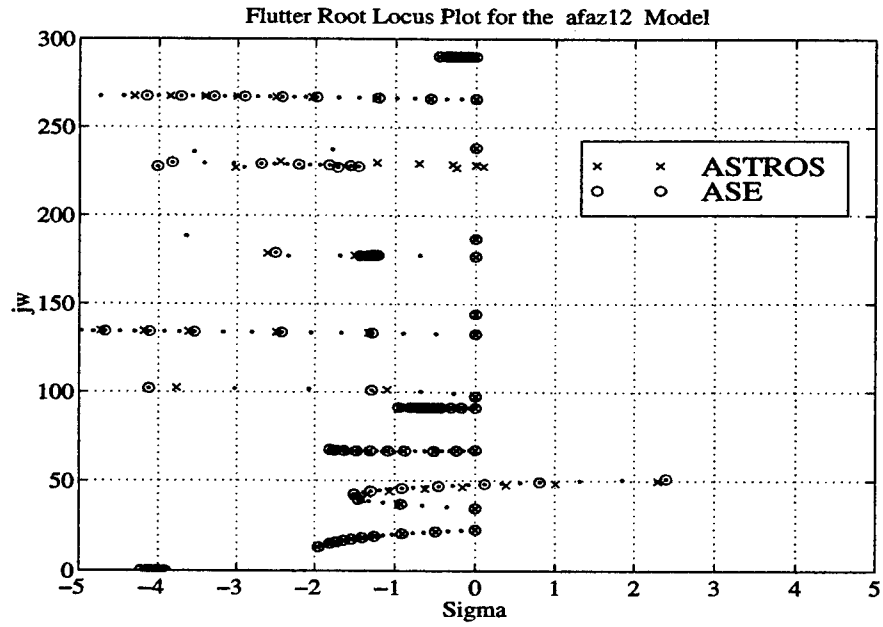


**Figure 18. ASTROS and ASE with MIST approximation (12 modes, 10 lags; upper plot - with constraints; lower plot - without constraints).**

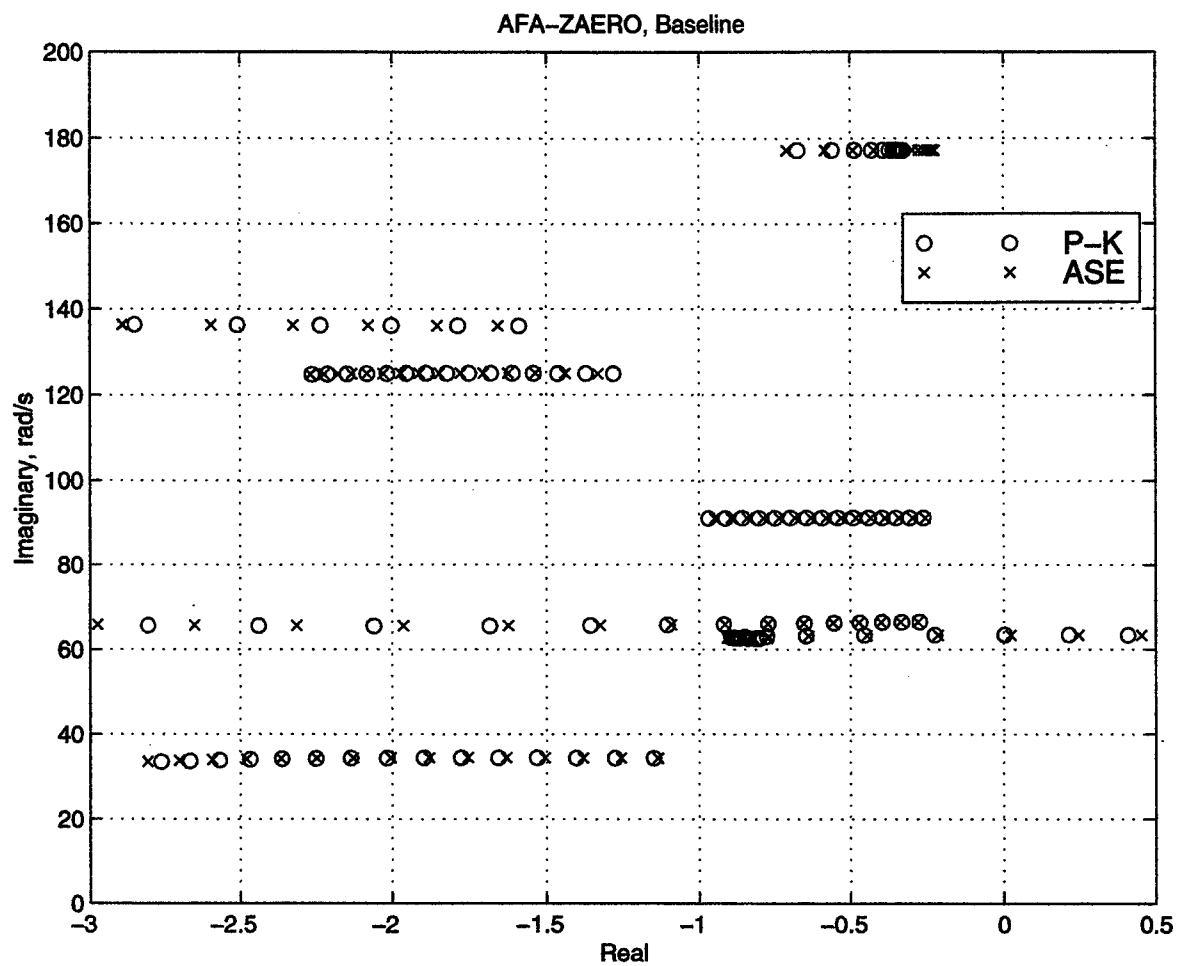


**Figure 19. Baseline flutter analysis.**

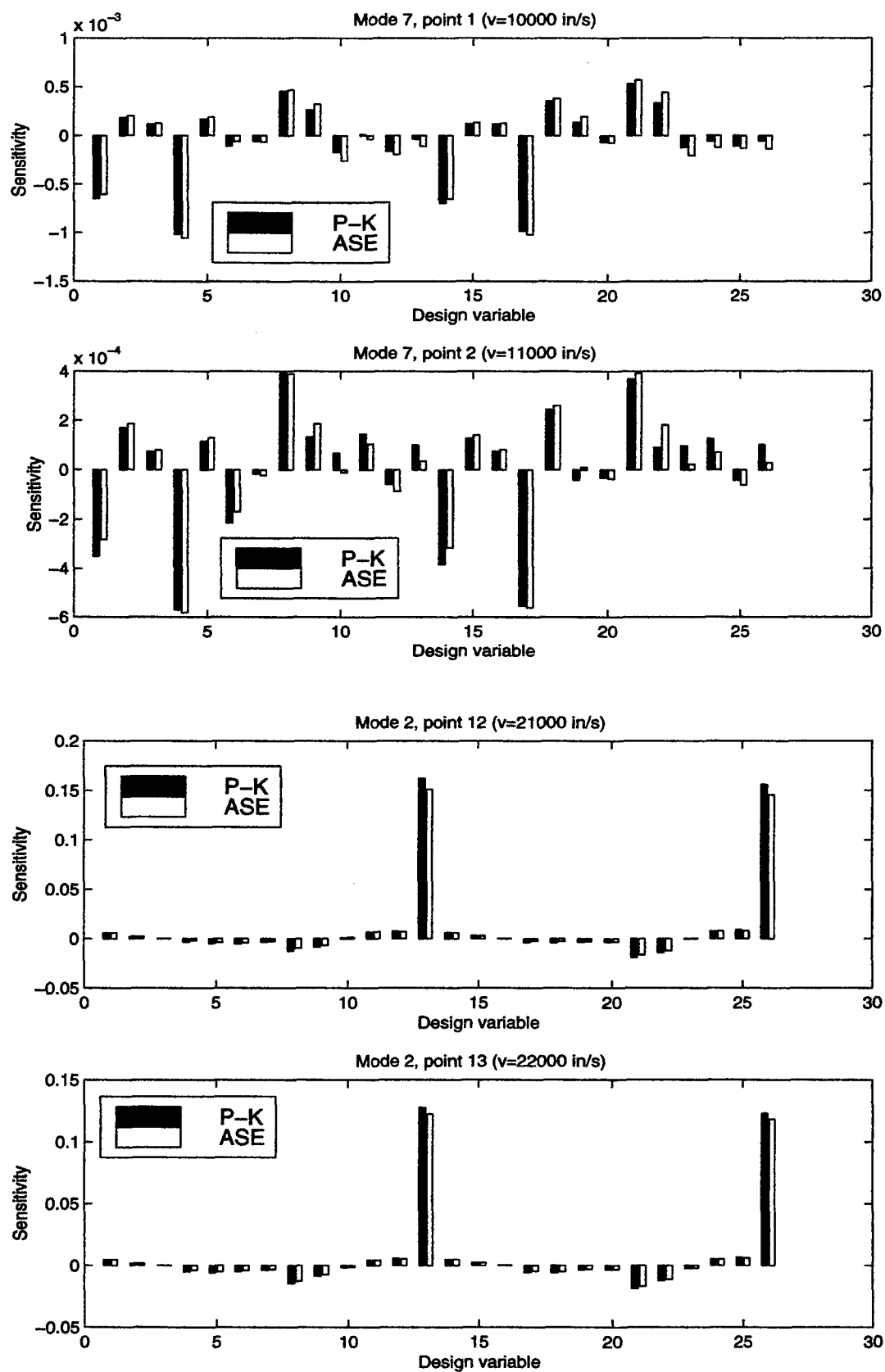


Figure 20. Baseline sensitivities of the flutter constraints.

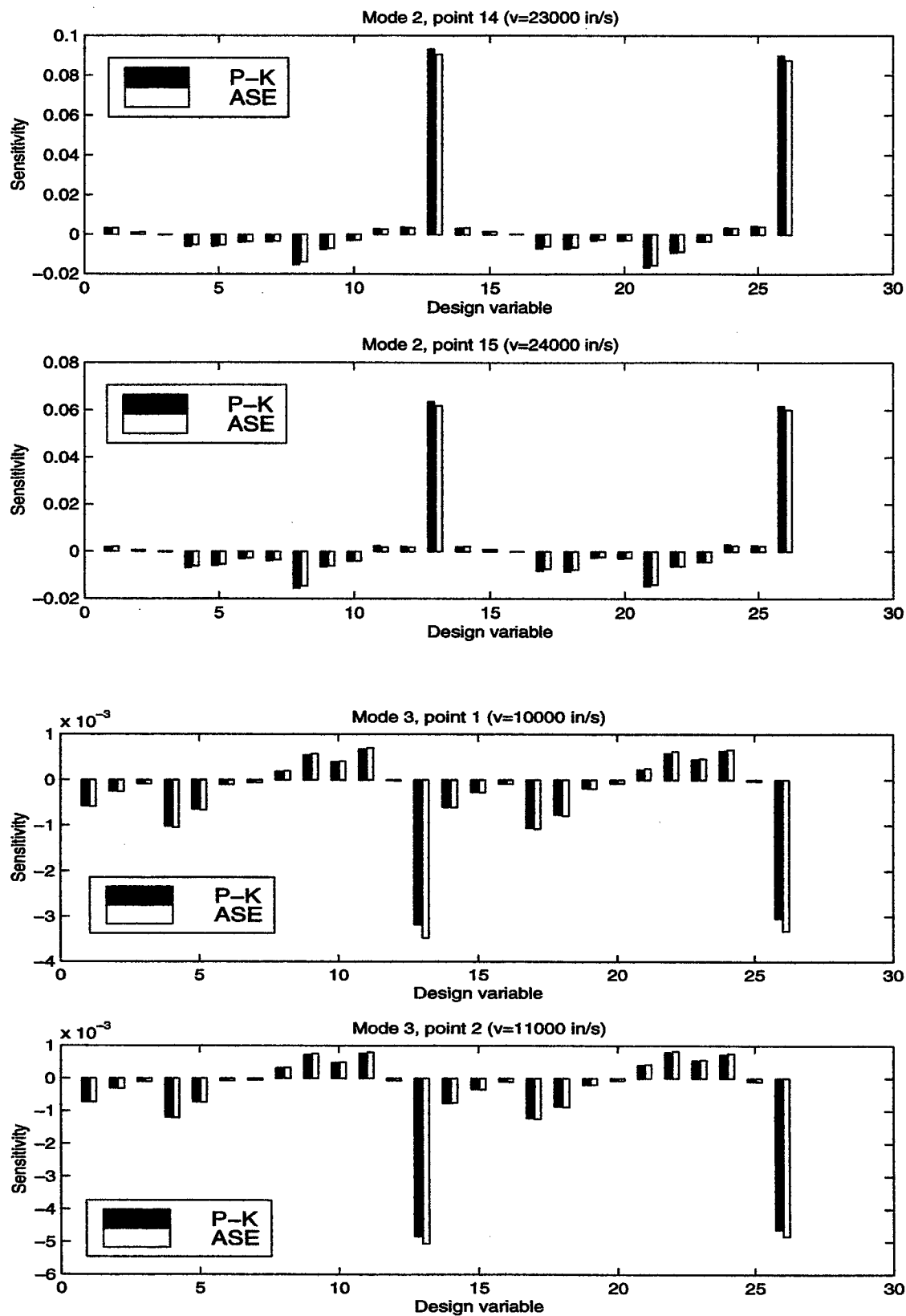


Figure 21. Baseline sensitivities of the flutter constraints.



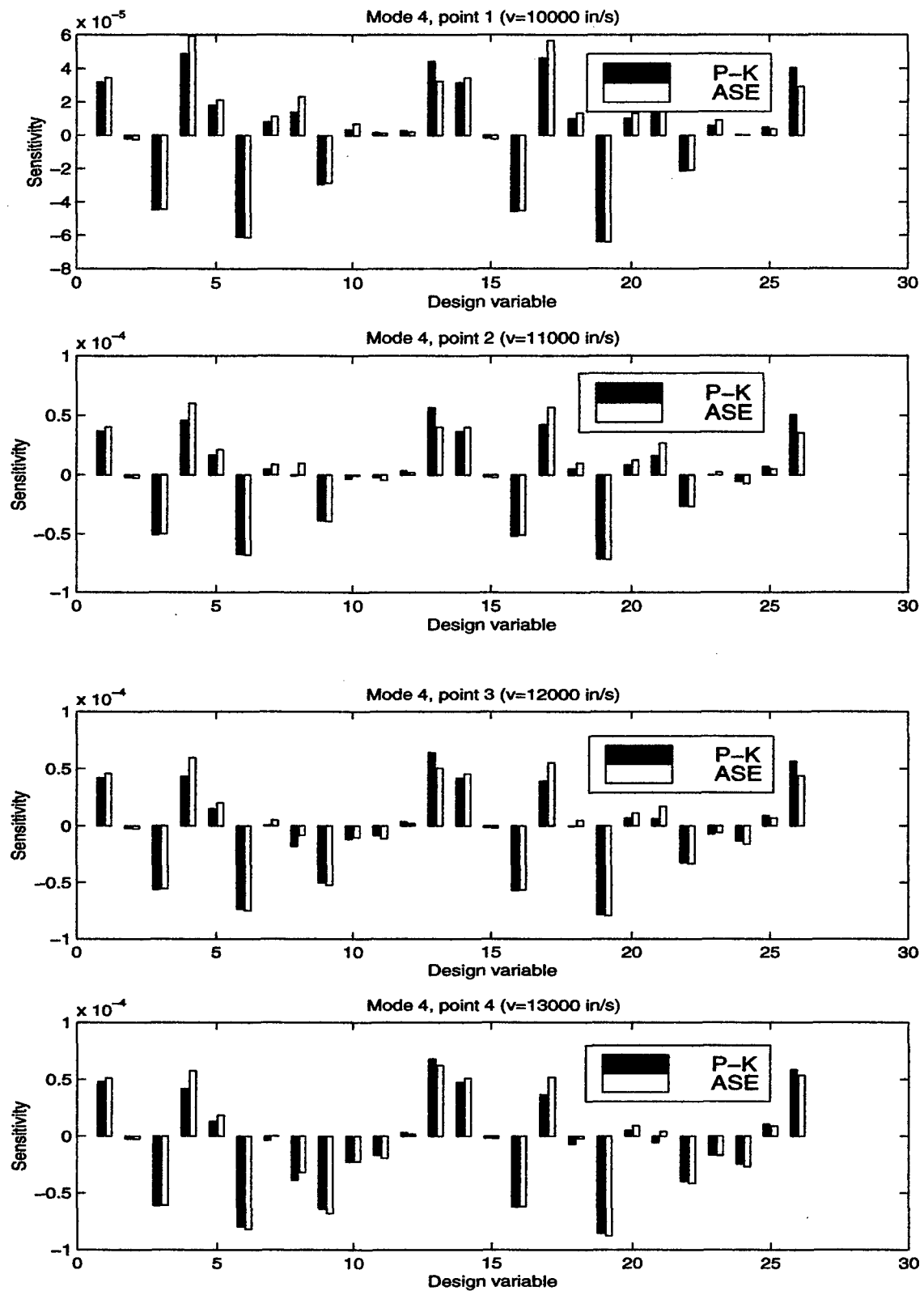


Figure 22. Baseline sensitivities of the flutter constraints.

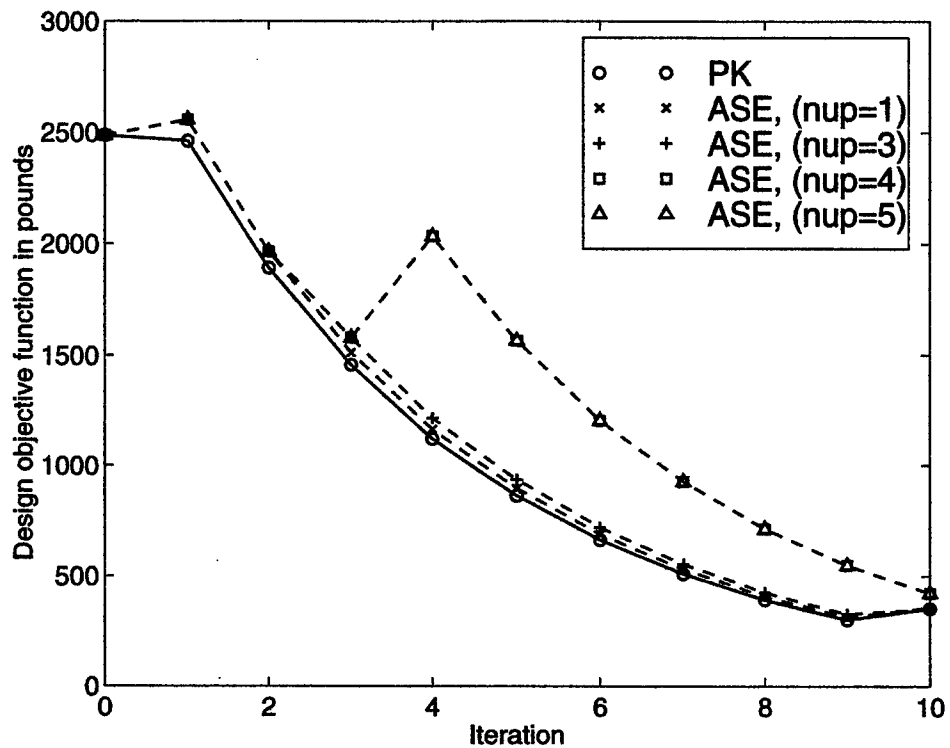


Figure 23. Optimization weight history (first iterations).

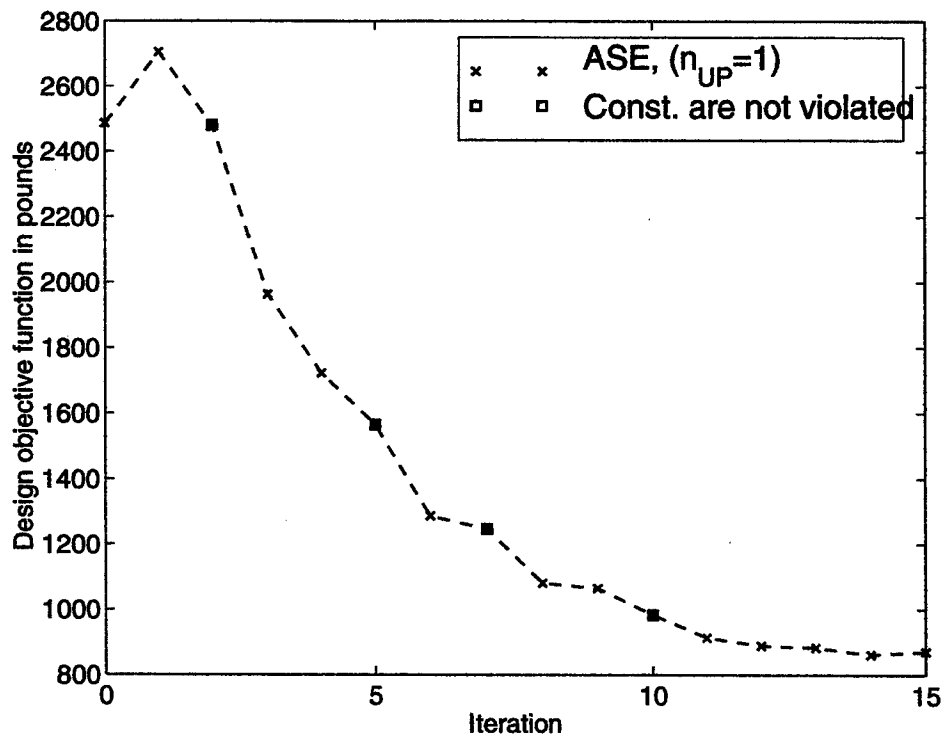


Figure 24. Optimization weight history (13 modes).

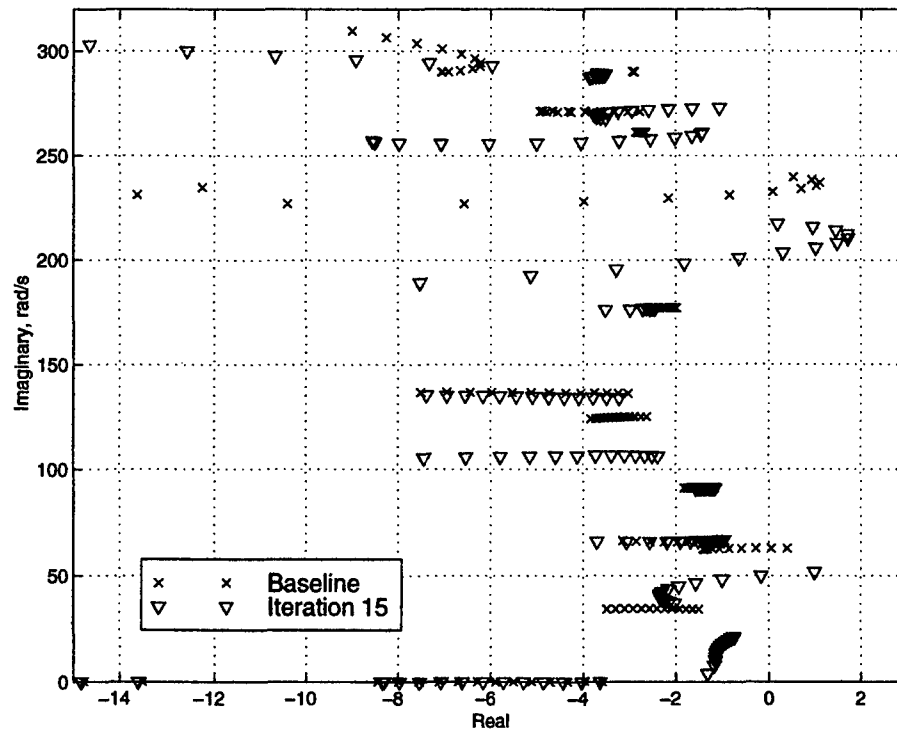


Figure 25. ASE flutter analysis (13 modes).

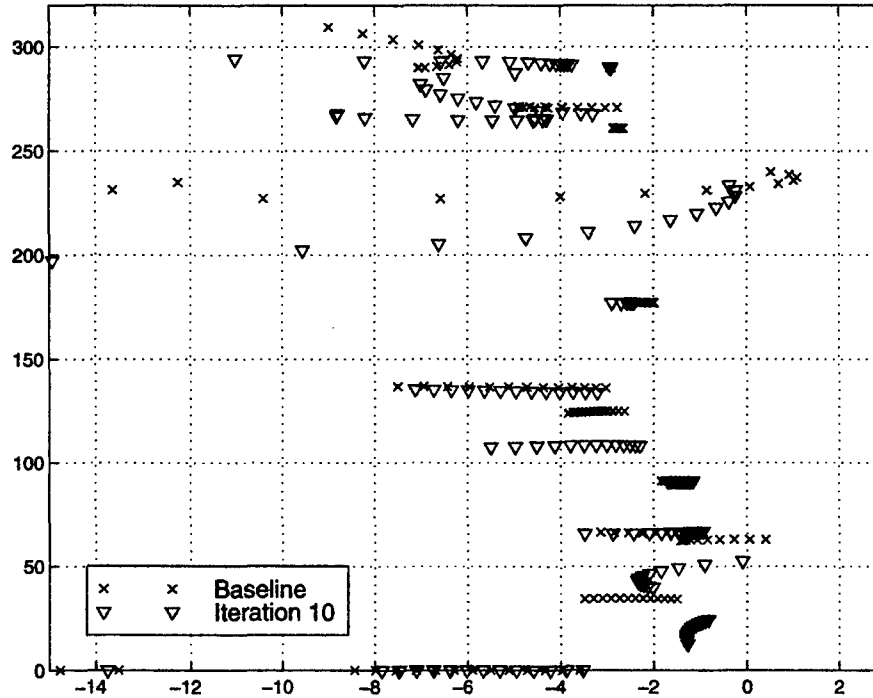


Figure 26. ASE flutter analysis (13 modes).

## **PART II: ASE OPTIMIZATION OF A FIGHTER AIRCRAFT USING ASTROZ**

### **1. Introduction**

This document contains the results of optimizations with flutter, control, and stress constraints using ASTROZ (ASTROS with ZAERO aerodynamics) and the new aeroservoelasticity (ASE) discipline. The application is to an advanced fighter aircraft (AFA) model.

### **2. Structural and Aerodynamic Models**

The aircraft structural model is shown in a different view in Figure 27. As in Part I, the subject for structural optimization was the skin of the wing torsion box (Figure 2). The design variables were again the thicknesses of the upper and lower skins in the 13 design zones, for a total of 26 structural design variables. Here, the initial design thicknesses for all the design variables were to 0.5 inches.

The same unsteady aerodynamic model as in Part I was used. It is shown in Figure 3 and described in Section I-2.

### **3. Control System**

A simple control system which relates the commands to the outboard and inboard actuators,  $u_{p1}$  and  $u_{p2}$ , to a single roll-rate signal,  $y_p$ , was used in the numerical application. A block diagram of the control system is shown in Figure 28. It includes a low-pass filter and two gains. The parameter  $G_3$  defines the low-pass filter bandwidth introduced to avoid high-frequency flutter/spillover.

A preliminary control synthesis with limited information on the aeroelastic system defined a baseline system with  $G_1 = 0.06$ ,  $G_2 = -0.3$ , and  $G_3 = 10$ . The gains were defined by ASEGAIN cards and declared as design variables by standard DESVARP cards that relate to standard ELIST cards with ID numbers equal to those of the associated ASEGAIN cards. Since we could not add new elements to the list of design variables, the variable gains were represented in the design by dummy CROD elements to be defined by the user. Each ELIST card must relate to a different dummy CROD element.

The dummy CROD elements were connected to dummy grid points, which were not part of the structure. All degrees of freedom of these grid points were clamped, such that there was no influence on the structural analysis. When the material density of the dummy rods was set to zero, the variable gains had no effect on the objective function. It is desirable in many cases to set a non-zero density of small value such that there is a penalty for large gains. The dummy rod weights were added in this case to the objective function.

#### 4. Flutter Constraints

Flutter constraints were applied for anti-symmetric boundary conditions at Mach 0.9. Thirty low-frequency modes, including one rigid-body mode, were used for updating the modal properties and performing ASE analysis during the optimization. Fourteen reduced frequency values between 0.0001 and 0.3 were used to create the aerodynamic database. The design velocity was defined as 12057. *inches/sec* at sea level. Flutter design points were defined at the nine velocity values of 7000.0, 8000.0, 9000.0, 10000.0, 11000.0, 12057.0, 13000.0, 14000.0, and 14470.0 *inches/sec*. Two additional values of velocity provided the required flutter margin. The structural damping was defined as  $g=0.02$  for all the modes. The flutter constraints required the damping to be positive at all of the design points.

#### 5. Control Constraints

The control constraints applied in the optimization were control-margin constraints and constraints on the open-loop aeroelastic system gain from control surfaces to a roll-rate sensor. The control margin constraints require specific gain- and phase-margin values at various velocities up to the design velocity of 12057 *inches/sec*. The upper gain margins were required to be more than 6 *dB*, there were no limits on the lower gain margins because they were irrelevant in this case. The upper phase margins were required to be more than 45 *degrees*, and the lower phase margins were required to be less than -45 *degrees*. The requirement for the open-loop aeroelastic system gain was

$$G_1 G_{p1} + G_2 G_{p2} \leq -G_{req}$$

where  $G_1$  and  $G_2$  are the outboard and inboard actuator input gains shown in Figure 28 and  $G_{p1}$  and  $G_{p2}$  are the aeroelastic gains from the actuators to the roll-rate sensor.

The differences between the optimization cases below consisted of the ways in which the aeroelastic gain constraints in this equation were applied.

#### 6. Stress Constraints

Stress constraints were applied for a 9g pull-up maneuver at Mach 0.95. The loads for this maneuver were calculated using the SAERO discipline of ASTROZ and were used in the STATICS discipline of the optimization process. Von-Misses stresses in all of the skin design variables were required to be less than 36700 *psi*.

#### 7. General Results of Optimizations

##### 7.1 Case 1: High aeroelastic gain requirement

The flutter, control, and stress constraints discussed above were applied with  $G_{req} = 4$  at all velocities up to 12060 *inches/sec* which dropped linearly down to  $G_{req} = 1$  at the velocity of 15000 *inches/sec*. This was found to be a high requirement, which drove the optimization to increase the structural weight.

The modal database was updated in this case every ten iterations  $n_{UP} = 10$ . The optimization weight history is given in Figure 29. The designed weight was increased by 6.99% from 779.5 *lbs* to 834.2 *lbs*.

The root loci for the baseline and final design structures are shown in Figure 30. It can be observed that flutter, which appeared in the second elastic mode in the baseline structure, disappeared in the final design.

The histories of the aeroelastic system gain, the positive gain margin, and the positive phase margin at the design velocity are shown in Figures 31 – 33. The histories of the controller gain factors (multiplying the baseline gains of 0.06, -0.3, and 10) are shown in Figure 34.

## 7.2 Case 2: Moderate aeroelastic gain requirement

The flutter, control, and stress constraints discussed above were applied with  $G_{req} = 3$  at all velocities up to 12060 *inches/sec* which dropped linearly down to  $G_{req} = 0.5$  at the velocity of 15000 *inches/sec*. Another change from Case 1 was the assignment of structural weight to the dummy CROD elements representing the variable control gains. With such an aeroelastic gain requirement, the total wing weight was reduced considerably.

The sensitivity of the CROD weights to a unit change in a gain factor was set to 0.1 *lbs*. The total added dummy weight due to the control gains was 0.3 *lbs* for the baseline structure and 0.2 *lbs* for the final design.

The optimization history is given in Figure 35. The designed weight was decreased from 779.51 *lbs* to 679.48 *lbs* (the fictitious weight of the gains was subtracted).

The root loci for the baseline and final design structures are shown in Figure 36.

The histories of the aeroelastic system gain, the positive gain margin, and the positive phase margin at the design velocity are shown in Figures 37 - 39. The histories of the controller gain factors are shown in Figure 40.

## FIGURES FOR PART II

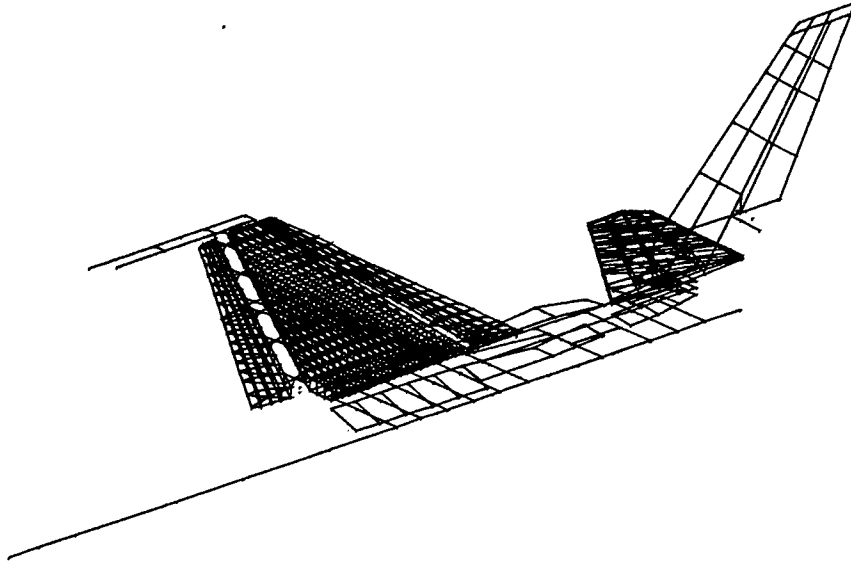


Figure 27. AFA structural model – different view.

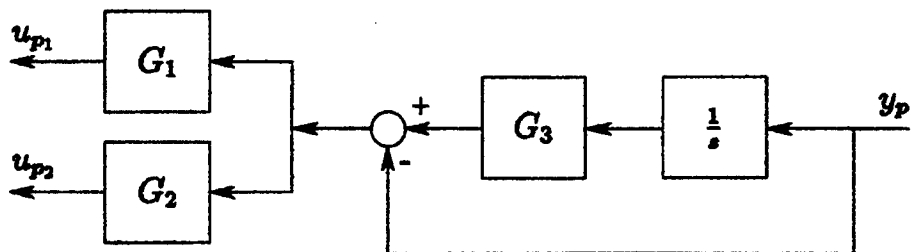


Figure 28. Control system interconnection model for the numerical example.

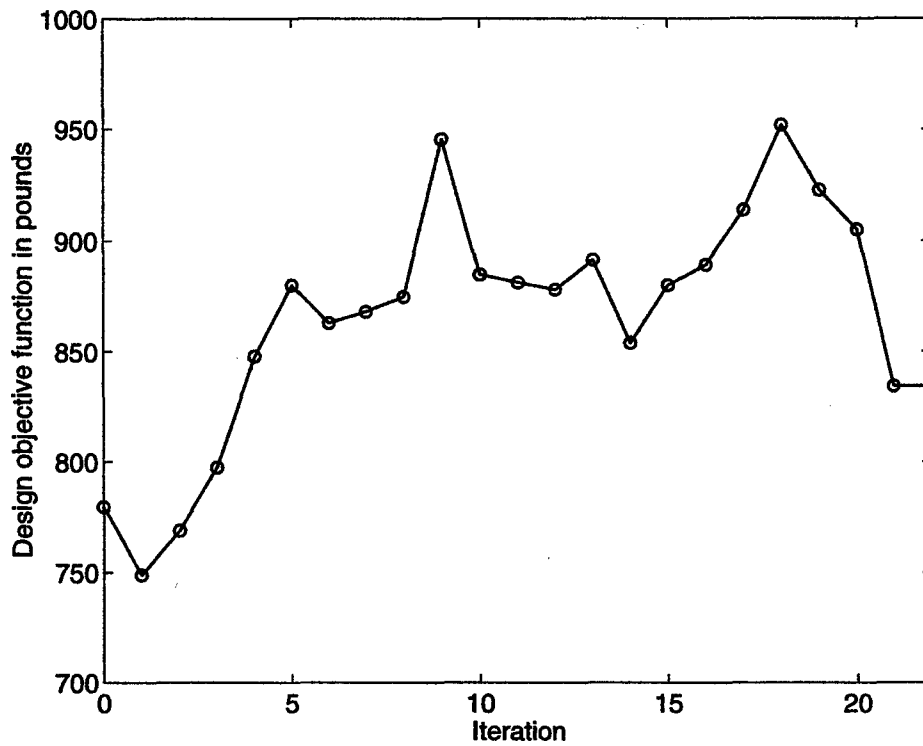


Figure 29. ASE optimization weight history (Case 1).

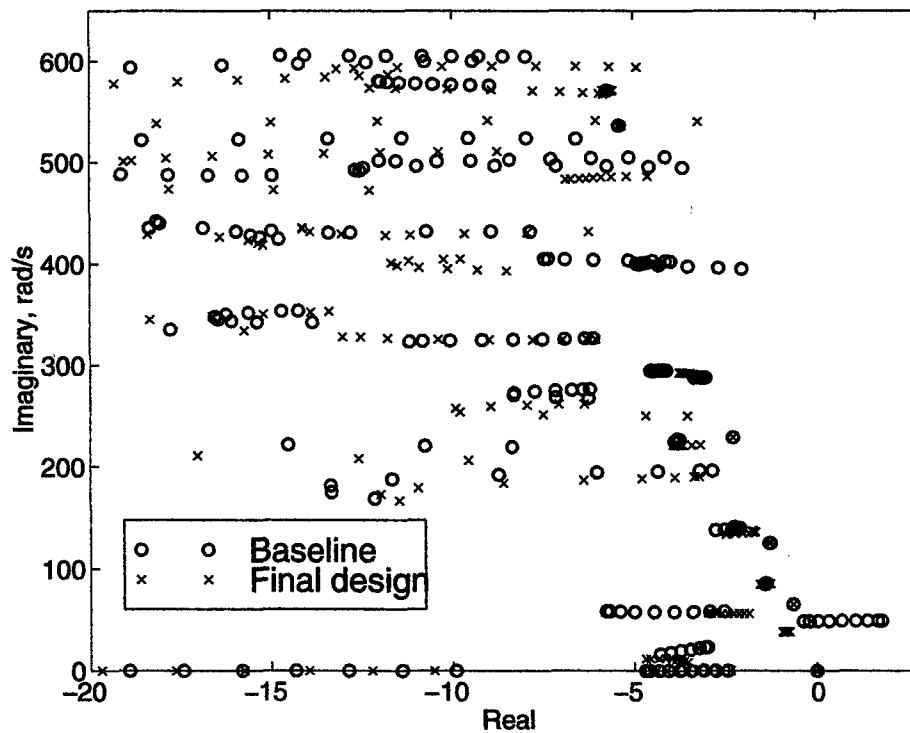
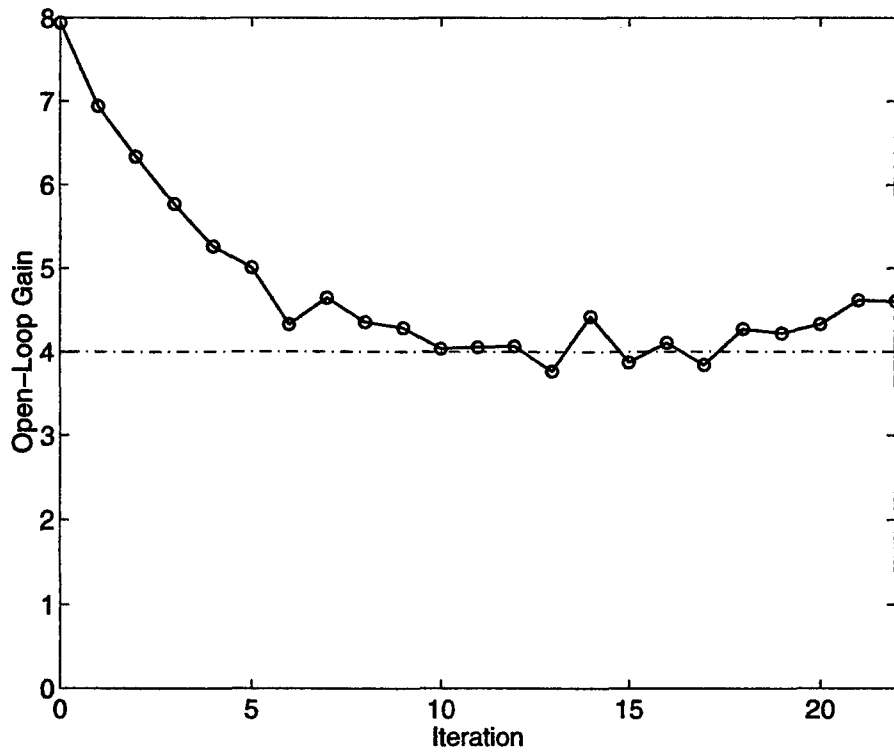
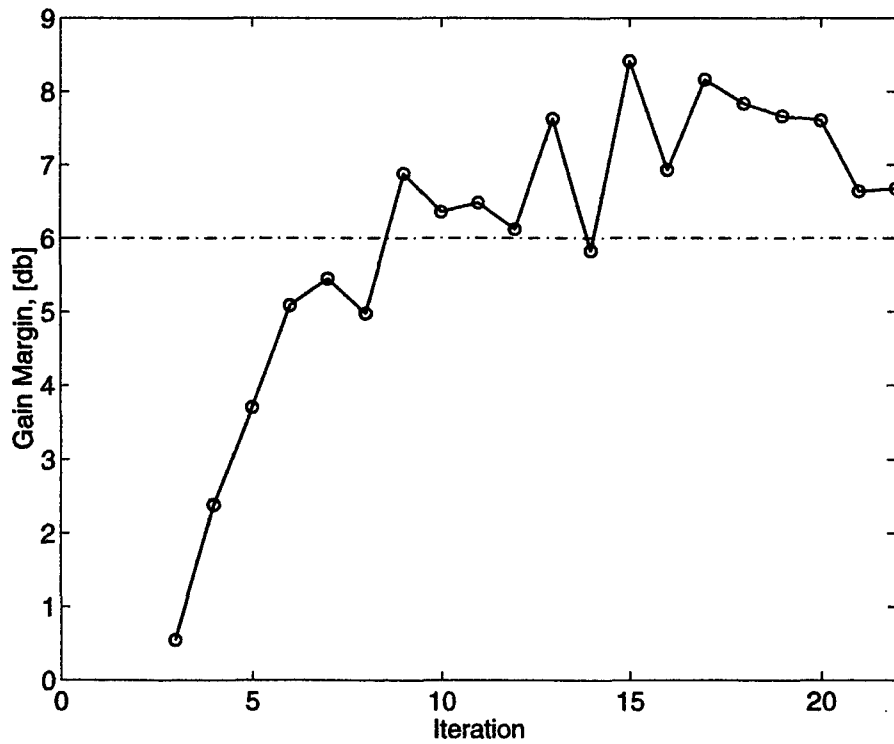


Figure 30. Root loci for the baseline and final design structures (Case 1)





**Figure 31. Aeroelastic system gain history (Case 1).**



**Figure 32. Positive gain margin history (Case 1).**

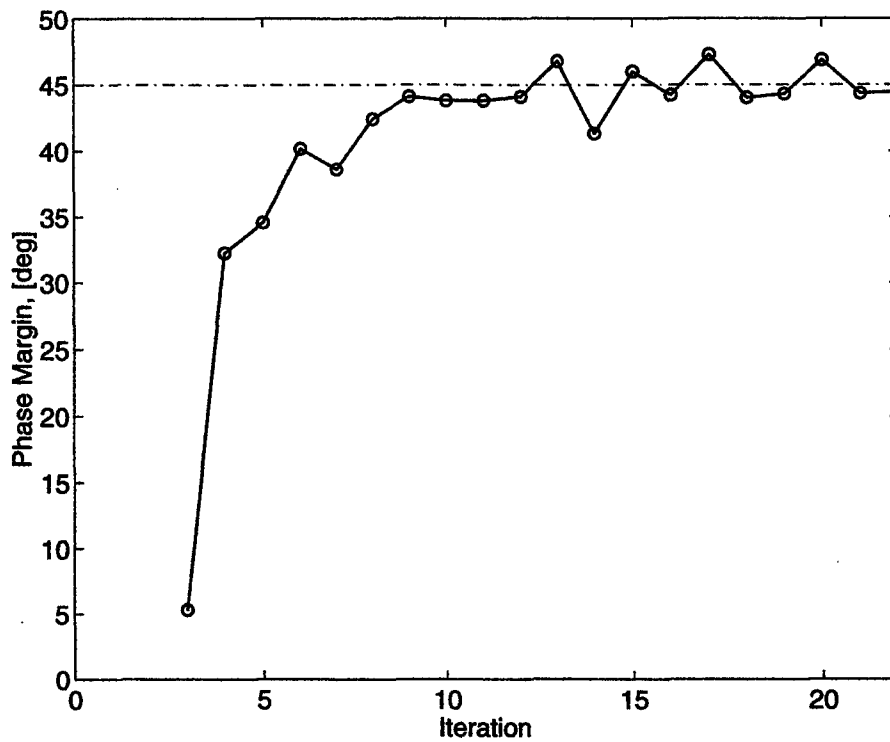


Figure 33. Positive phase margin history (Case 1).

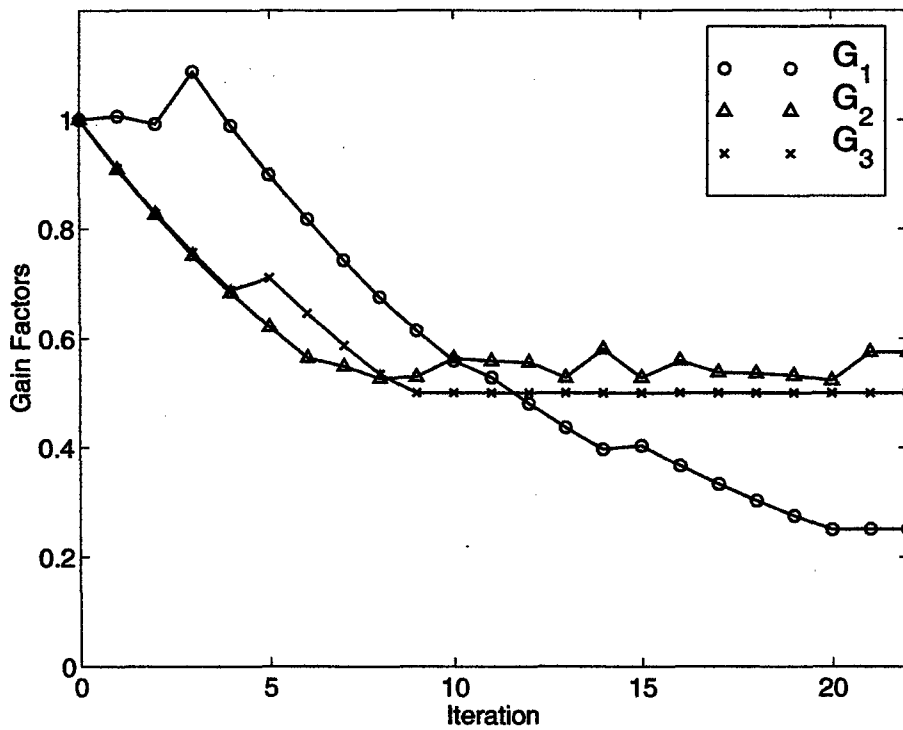


Figure 34. Histories of controller gain factors (Case 1).

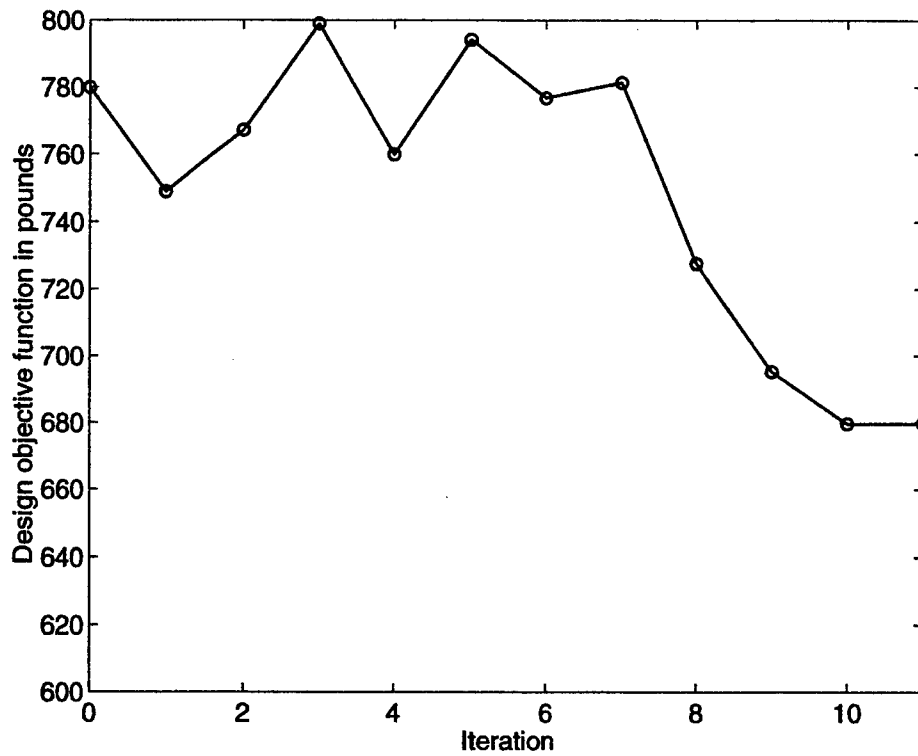


Figure 35. ASE optimization weight history (Case 2).

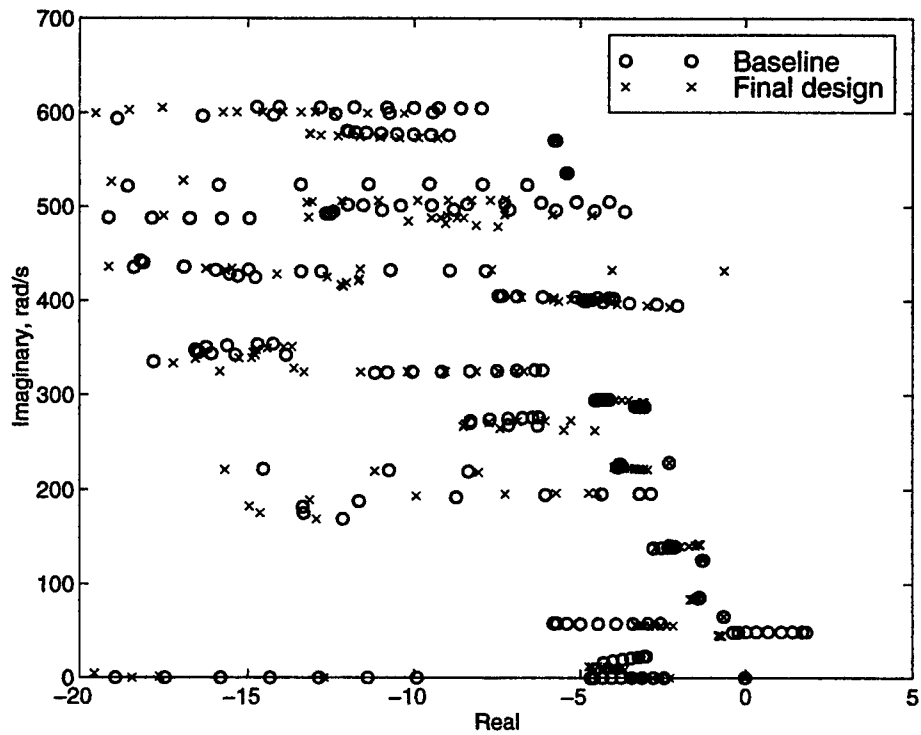


Figure 36. Root loci for the baseline and final design structures (Case 2).

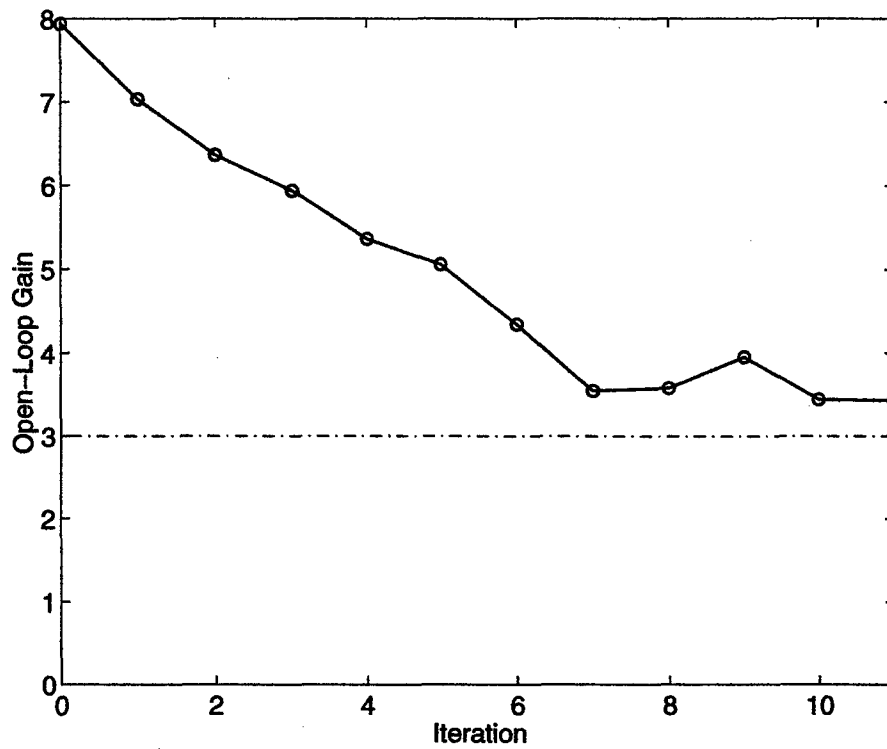


Figure 37. Aeroelastic system gain history (Case 2).

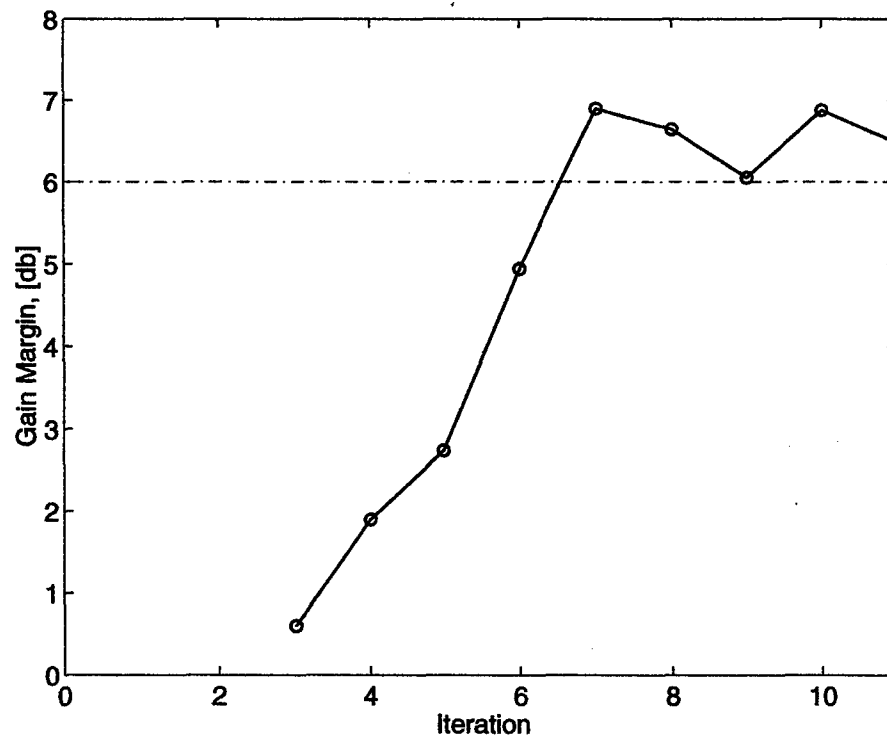


Figure 38. Positive gain margin history (Case 2).

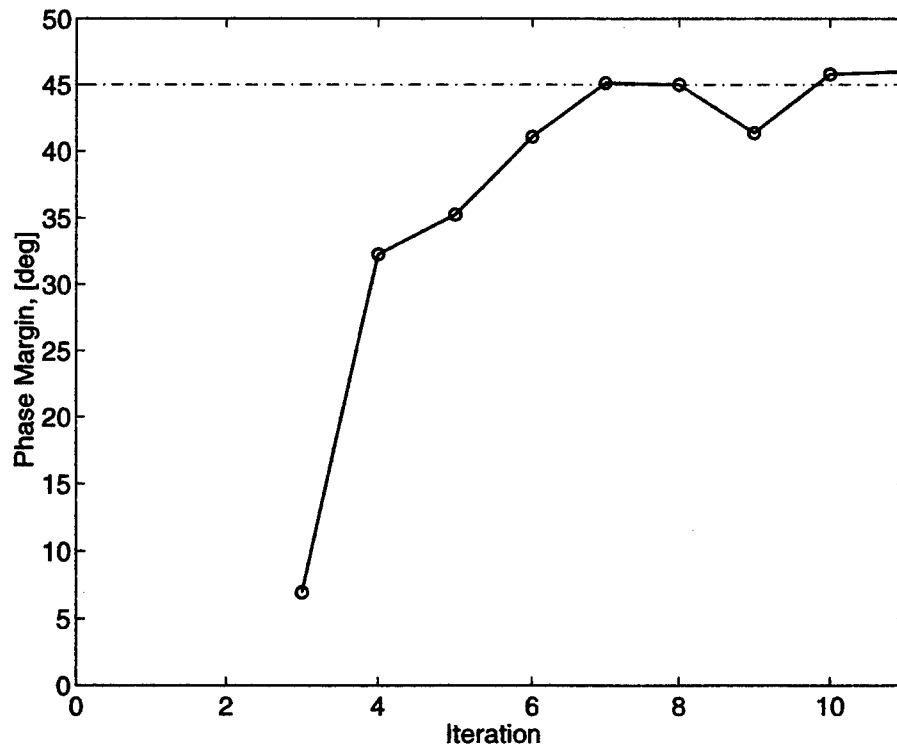


Figure 39. Positive phase margin history (Case 2).

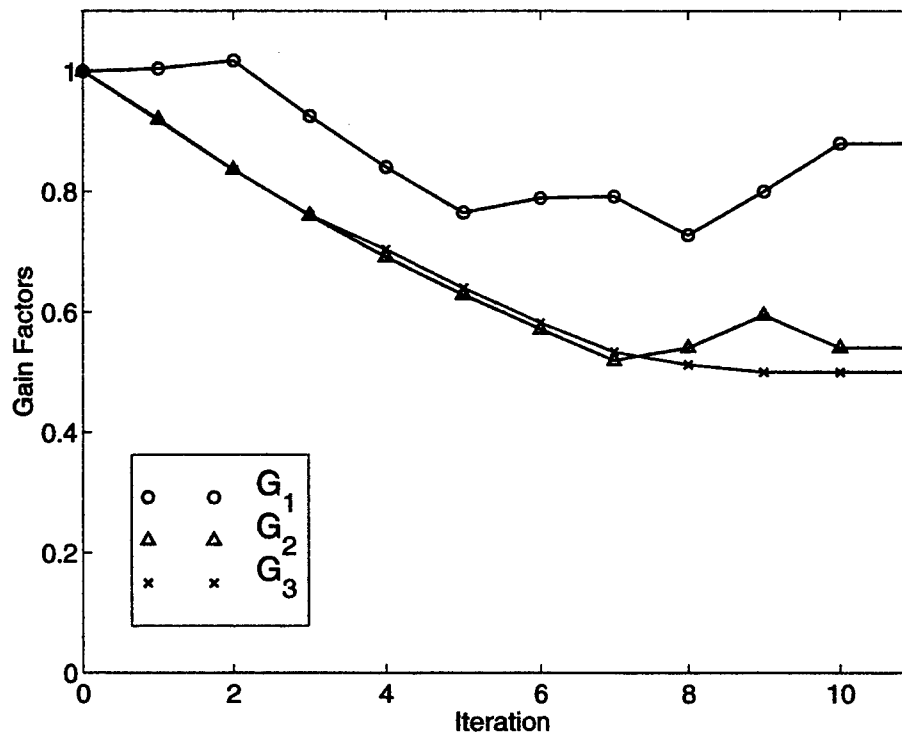


Figure 40. Histories of controller gain factors (Case 2).